Copy No. ____

Defence Research and Development Canada
Recherche et développement pour la défense Canada

DEFENCE R&D DÉFENSE

DSSP50 Build 090910 Documentation

Part 3: Algorithm Description

M. Mackay

Defence R&D Canada – Atlantic

Technical Memorandum
DRDC Atlantic TM 2009-228
December 2009

Canada

This page intentionally left blank.

DSSP50 build 090910 Documentation, Part 3: Algorithm Description

M. Mackay
Defence R&D Canada – Atlantic

Defence R&D Canada – Atlantic
Technical Memorandum
DRDC Atlantic TM 2009–228
December 2009

Author

Original signed by M. Mackay

M. Mackay
Defence Scientist

Approved by

Original signed by N. Pegg

N. Pegg
Head, Warship Performance

Approved for release by

Original signed by R. Kuwahara for

C. Hyatt
Chair, Document Review Committee

© Her Majesty the Queen as represented by the Minister of National Defence, 2009
© Sa majesté la reine, représentée par le ministre de la défense nationale, 2009

Abstract

DSSP50 is a computer code for evaluating the dynamics and manoeuverability of submarines and smaller streamlined underwater vehicles. This document is a description of the algorithms used in the program. Although written for DSSP50, it may be useful to those with a more general interest in simulating submarine manoeuvers. Other documents provide a guide to using DSSP50 and detail its input requirements.

Résumé

DSSP50 est un code machine permettant d'évaluer la dynamique et la manœuvrabilité des sous-marins et des plus petits véhicules sous-marins hydrodynamiques. Le présent document est une description des algorithmes utilisés logiciel. Quoiqu'il ait été écrit pour le DSSP50, il peut être utile à ceux ayant un intérêt plus général à la simulation des manœuvres des sous-marins. D'autres documents fournissent un guide à l'utilisation du DSSP50 et donnent les détails de ses exigences d'entrée.

This page intentionally left blank.

Executive Summary

DSSP50 build 090910 Documentation, Part 3: Algorithm Description
M. Mackay; DRDC Atlantic TM 2009–228; Defence R&D Canada – Atlantic; December 2009.

Introduction: DRDC Submarine Simulation Program, version 5.0 (DSSP50), was developed to predict the manoeuverability of submarines and smaller underwater vehicles. It combines the capability of two earlier codes, DSSP21 and DSSP40. The program is used to calculate loads on captive models, derive hydrodynamic coefficients, simulate tactical manoeuvers, and generate Manoeuvering Limitation Diagram (MLD) curves.

This document is a description of the algorithms in DSSP50. Its principal objective is to provide background for the DSSP50 user guide and input reference, but it may also be read as a general discussion of modeling submarine hydrodynamics and systems for fast simulation methods.

Significance: The target user group for the program is DRDC and other Government researchers, CF engineers, and CF contractors.

DSSP50 was formulated to balance accuracy, which is sufficient for predicting complex tactical manoeuvers, with computational speed. Speed is required for systematic studies in support of preliminary design and for MLD calculations. Making it multifunctional ensured that all calculations and simulations are based on a common set of algorithms, and thus consistent.

Although input to the program initially appears complex because of a large number of options, experience with its predecessors suggests that it should be relatively easy to learn. This document will help identify which of the program options are appropriate for a particular problem.

Future Development: Future development may include such features as near-bottom operation.

Sommaire

DSSP50 build 090910 Documentation, Part 3: Algorithm Description
M. Mackay; DRDC Atlantic TM 2009–228; R & D pour la défense Canada – Atlantique; décembre 2009.

Introduction: Le logiciel de simulation sous-marine de RDDC, version 5.0 (DSSP50), a été développé afin de prévoir la manœuvrabilité des sous-marins et des véhicules sous-marins plus petits. Il combine la capacité de deux codes antérieurs, DSSP21 et DSSP40. Le logiciel sert au calcul des charges sur des maquettes entravées, à calculer les coefficients hydrodynamiques, à simuler les manœuvres tactiques et à générer des courbes des schémas de limitation des manœuvres (SLM).

Le présent document est une description des algorithmes utilisés dans DSSP50. Son objectif principal est de fournir un contexte pour le guide utilisateur et la référence d'entrée du DSSP50, mais il peut également être lu en tant que discussion générale de la modélisation de l'hydrodynamique et des systèmes des sous-marins pour des méthodes de simulation rapide.

Portée: Le groupe utilisateur cible pour le logiciel est RDDC et d'autres chercheurs du gouvernement, les ingénieurs des FC et les entrepreneurs des FC.

Le DSSP50 a été formulé pour équilibrer la précision, qui est suffisante pour prévoir des manœuvres tactiques complexes, à la vitesse computationnelle. La vitesse est requise pour des études systématiques de soutien à la conception préliminaire et aux calculs des SLM. Le fait de le rendre multifonctionnel a permis de garantir que tous les calculs et les simulations sont basés sur un ensemble commun d'algorithmes et sont ainsi compatibles.

Quoique l'entrée dans le logiciel semble initialement complexe compte tenu du grand nombre d'options, l'expérience avec ses prédécesseurs donne à penser qu'elle devrait être relativement facile à apprendre. Le présent document aidera à déterminer quelles options du logiciel sont appropriées à un problème particulier.

Recherches futures: Les recherches futures pourraient comprendre des caractéristiques comme les opérations près du fond.

Table of Contents

Abstract i
Résumé i
Executive Summary iii
Sommaire iv
Table of Contents v
List of Figures vii
List of Tables vii
1 Introduction 1
2 Vehicle Equations of Motion 2
2.1 Dynamics 2
2.2 Hydrodynamic Loads 4
2.3 Component Based Models 4
2.4 Coefficient Based Models 5
2.5 DSSP50 6
3 Axis Systems 6
4 Hull Component Loads 6
4.1 HulFor Calculations 7
4.2 Empirical Predictions 8
4.3 Jeans Method 8
4.4 Keel and Deck 10
4.5 Hull Drag 10
5 Appendage Component Loads 11
5.1 Summary of Appendage Load Prediction 12
5.2 Tailplane Efficiency 18
6 Out-of-Plane Loads 21
7 Lump Loads 22
8 Propulsion 24
9 Control Deflection Dynamics 26
10 Autopilots 26
11 Plane Reversal 29
12 Compression 30
13 Blowing Main Ballast 30
14 Compartment Flooding 34
15 Trim and Compensation 35
16 Variable Mass 35

17 Integrating the Equations of Motion 36
17.1 The State Variable Equations 36
17.2 Inverting the I+A Matrix 39
17.3 Trajectory and Attitude 39
17.4 Integration Methods 42
18 MLD Curve Simulation 43
19 Concluding Remarks 45
References 47
Nomenclature 51
Distribution 57

List of Figures

Figure 1.	Principal earth-fixed and boat-fixed axis systems	7
Figure 2.	Comparison between in-plane load data and predictions	9
Figure 3.	The effect of a keel and deck on sideforce	10
Figure 4.	Hull/sail parameter nomenclature	13
Figure 5.	Endplate parameter nomenclature	14
Figure 6.	Flapped appendage parameter nomenclature	14
Figure 7.	Sail and deck casing parameter nomenclature	15
Figure 8.	Sailplane parameter nomenclature	16
Figure 9.	Geometry for the Bohlmann/Spreiter Method	19
Figure 10.	Incremental normal force *vs* pitch angle for three hull-appendage configurations	20
Figure 11.	The effect of pitch/diameter ratio on Wageningen B4–70 propeller series data	25
Figure 12.	Autopilot response to two short error signals	28
Figure 13.	Plane reversal compensation	29
Figure 14.	Compression parameters	30
Figure 15.	A comparison between blowing models	34
Figure 16.	The centroid of floodwater in a watertight compartment	35
Figure 17.	Schematic Manoeuvering Limitation Diagram	44

List of Tables

Table 1.	Appendage load parameter dependence	17
Table 2.	System of equations integrated in a free manoeuver or MLD simulation	43

This page intentionally left blank.

1 Introduction

Computer program DSSP50 evaluates the hydrodynamics and manoeuverability of underwater vehicles. It is primarily for submarines although it can be applied to smaller streamlined submersibles. Hydrodynamic loads on the vehicle are calculated with a mix of fast semiempirical and coefficient based methods. Speed is necessary for systematic parameter variation during preliminary design, for evaluating emergency recovery procedures, and for other applications requiring many simulation runs.

DSSP50 documentation is in three parts:

- A general program guide, reference [1], primarily for new users.
- An input reference, reference [2], for all users.
- A description of the algorithms, this memorandum, for background information.

After some familiarity with the program is acquired, the principal resource will be the input reference.

The purpose of this memorandum is to outline DSSP50 algorithms and numerical methods in order to increase understanding of the program for users and code maintainers alike. It may also be of interest to a wider audience since in a number of aspects it can be read as a general discussion of simulating submarine manoeuvers. However, because this is within the context of DSSP50 the general reader should be aware that selection and implementation of any particular numerical model may have been influenced by other requirements and features of the program.

The normal release of DSSP50 comprises a Windows executable **dssp50.exe** with the run-time library `salflibc.dll` and some other files including those created by the author for the tutorial.

Developmental status of the code is indicated by a build number consisting of the release date in *yymmdd* format. (In output from the program, an additional character may be appended: `A`, `B`, or `X`, indicating that the build is considered to be a preliminary, limited, or experimental release respectively. After sufficient validation the qualifier will be dropped.) The build at time of writing is 090910; subsequent builds will be accompanied by updates and additions to the documentation as required.

The program proceeds in two phases:

- Vehicle model and systems setup. The user must provide a file defining the vehicle geometry or hydrodynamic coefficients, or a combination of the two, together with basic systems information. The data is extensively checked and as much preprocessing of it is done as possible.
- Hydrodynamic and manoeuvering simulations. The simulations to be run are defined in sequence on an optional input file. Simulations include static and dynamic loads on a captive vehicle, hydrodynamic coefficient generation, free vehicle manoeuvering, and Manoeuvering Limitation Diagram (MLD) curve calculation. If the simulation input file is absent, there is no work done in the second phase.

The objective in making the program multifunctional was to base all calculations and simulations on a common set of hydrodynamic modeling subroutines. The underlying hydrodynamic models are therefore consistent, and improvements and enhancements to the models will be applied universally.

DSSP50 is programmed in Fortran. Some parts of it are from much earlier programs, other parts are quite new. The code was revised to compile under Fortran 95 syntax rules, but only a handful of features are unlikely to compile under Fortran 77. One feature, the library routine required to extract the optional command line parameter, is compiler-dependent. DSSP50 was developed on a Microsoft Windows PC using the Salford FTN95 Win32 version 2.00 compiler, and checked with STI's Understand for Fortran, version 1.4. Although the code is virtually platform-independent, the documentation assumes a Windows platform where relevant.

The following conventions in the documentation should be noted. Object names (program units, etc.) and DSSP50 keywords are in a capitalized typewriter font. In discussing input, higher level keywords [1] following a lower level one are indicated by an arrow: `Lower` → `Higher`. The words 'simulation' and 'run' are generally synonymous except for an MLD simulation which comprises a number of individual runs.

2 Vehicle Equations of Motion

This section will outline the underwater vehicle equations of motion, including such restricted cases as simulation of static tests with a captive model. One way to characterize hydrodynamic modeling in a simulation is how the loads on the vehicle are calculated. DSSP50 combines the component based (or geometrical) approach with the more conventional coefficient based approach.

2.1 Dynamics

A manoeuvering submarine or submersible, at either full or model scale, is conventionally regarded as a rigid body moving in an earth fixed inertial reference frame. Its dynamics are governed by Newton's second law of motion:

$$\frac{d\mathbf{L}}{dt} + \mathbf{\Omega} \times \mathbf{L} = \mathbf{Q} \tag{1}$$

where $\mathbf{L}$ is the vector linear or angular momentum, $\mathbf{\Omega}$ is the vector angular velocity, and $\mathbf{Q}$ is the corresponding vector external load.

This is expressed in vehicle-fixed axes as a system of six equations of motion — one for each degree of freedom: surge, sway, heave, roll, pitch, and yaw. For example, the heave equation, expanding the left hand side of the previous equation for an arbitrary axis origin, is [3]:

$$m\left[\dot{w} - uq + vp - x_G\left(\dot{q} - rp\right) + y_G\left(\dot{p} + qr\right) - z_G\left(p^2 + q^2\right)\right] \;=\; Z \tag{2}$$

and the pitch equation is:

$$I_y\dot{q} - (I_z - I_x)rp - I_{yz}(\dot{r} - pq) - I_{xy}(\dot{p} + qr) - I_{xz}\left(r^2 - p^2\right) + m\left[z_G(\dot{u} - vr + wq) - x_G(\dot{w} - uq + vp)\right] = M \quad (3)$$

where $(m, I_x, \ldots)$ are the vehicle inertial properties, $(u, v, w, p, q, r)^T$ is a partial state vector comprising translational and rotational velocities, and (x_G, y_G, z_G) is location of the vehicle CG. Z is normal force and M is pitching moment. For the moment we are assuming that the inertial properties are constant with respect to time, otherwise additional terms will appear in the equations. Section 17 presents all six of the equations of motion in more detail together with the derivation of trajectory and attitude.

Consider the right hand side of equation (1). External forces and moments arise from added masses and moments, from hydrodynamic reactions, from gravity and buoyancy, from propulsors, and, in the case of the captive model, from balance reactions. In the absence of near-surface effects, added masses and moments are constant with respect to time for a subsurface vehicle, and, in terms of the extended state vector $\mathbf{u} = (u, \ldots, r, \phi, \theta, \psi, \delta, \ldots)^T$, the equations of motion can be expressed as:

$$(\mathbf{I} + \mathbf{A})\dot{\mathbf{u}} = \mathbf{T}(\mathbf{u}) + \mathbf{F}(\mathbf{u}) + \mathbf{G}(\mathbf{u}) + \mathbf{P}(\mathbf{u}) + \mathbf{S} \quad (4)$$

in which $\mathbf{I}$ is the inertial properties matrix, $\mathbf{A}$ is the added mass and moment matrix, $\mathbf{T}$ is the axis rotational term (muq etc.), $\mathbf{F}$ is the hydrodynamic load term, $\mathbf{G}$ is the gravity and buoyancy term (including flooding and ballast blowing), $\mathbf{P}$ is the propulsion term, and $\mathbf{S}$ is the balance term. Additional terms may be present to account for directly-applied external forces such as those of the tow on a towed body. In the extended state vector, ϕ, θ, ψ are the Euler angles (we shall see in section 17.3 that other attitude parameters are preferable in the calculations) and δ denotes a generic control surface deflection.

Equation (4) is entirely general, and can be reduced to specific cases of interest. For a free swimming vehicle the balance term is omitted:

$$(\mathbf{I} + \mathbf{A})\dot{\mathbf{u}} = \mathbf{T}(\mathbf{u}) + \mathbf{F}(\mathbf{u}) + \mathbf{G}(\mathbf{u}) + \mathbf{P}(\mathbf{u}) \quad (5)$$

With the remaining terms in equation (5) prescribed, it can be integrated in time to obtain histories of the state variables $u, \ldots, r$, and the vehicle trajectory and attitude resulting from control deflections and other inputs.

For captive dynamic model test simulations the propulsion term is generally not required:

$$\mathbf{S} = (\mathbf{I} + \mathbf{A})\dot{\mathbf{u}} - \mathbf{T}(\mathbf{u}) - \mathbf{F}(\mathbf{u}) - \mathbf{G}(\mathbf{u}) \quad (6)$$

In this case the state vector and its time derivative, $\mathbf{u}$ and $\dot{\mathbf{u}}$, are prescribed, and the object is to estimate the balance forces and moments, $\mathbf{S}$.

For static test simulations the state vector time derivative is zero; $\mathbf{T}$ is retained for the case of constant rotation and is omitted otherwise:

$$\mathbf{S} = -\mathbf{T}(\mathbf{u}) - \mathbf{F}(\mathbf{u}) - \mathbf{G}(\mathbf{u}) \quad (7)$$

2.2 Hydrodynamic Loads

In general the right hand terms in equations (5) to (7), except for the hydrodynamic forces and moments, $\mathbf{F}(\mathbf{u})$, are relatively easy to estimate. For example, the inertial properties are measured, or derived from a detailed CAD representation of the vehicle, and the added masses and moments of its components can be calculated analytically for equivalent ellipsoids, with varying degrees of elaboration [4].

There are a number of different semiempirical approaches for formulating $\mathbf{F}(\mathbf{u})$, each offering a trade-off between computational effort, physical insight, and accuracy. DSSP50 uses both component based and coefficient based models.

2.3 Component Based Models

A component based model breaks down the vehicle into a reasonably small number of components whose individual and interactive hydrodynamics can be estimated. It can also be characterized as geometry or physics based, although some degree of empiricism is usually involved.

For just two components, subscripted 1 and 2:

$$\mathbf{F}(\mathbf{u}) = \mathbf{C}_1(\mathbf{u}) + \mathbf{C}_2(\mathbf{u}) + \mathbf{C}_{1,2}(\mathbf{u}) + \mathbf{C}_{2,1}(\mathbf{u}) \tag{8}$$

where $\mathbf{C}_1(\mathbf{u})$ and $\mathbf{C}_2(\mathbf{u})$ are the individual loads on each component and $\mathbf{C}_{1,2}(\mathbf{u})$ and $\mathbf{C}_{2,1}(\mathbf{u})$ are the interactions of each with the other. It is implied that each of these terms is estimated or measured in a local axis system for local flow and then transformed into vehicle axes before summation. A multi-component vehicle model is generally limited to two-component interactions:

$$\mathbf{F}(\mathbf{u}) = \sum_i \mathbf{C}_i(\mathbf{u}) + \sum_i \sum_{j, j \neq i} \mathbf{C}_{i,j}(\mathbf{u}) \tag{9}$$

Terms in equation (9) are typically in the form of semiempirical equations derived from a broad range of data [5,6]. Lookup tables or other parameter based estimates can also be used. If the individual terms are significantly nonlinear, this should be reflected in nonlinearity of the interaction terms. In all cases, the range of applicability of the underlying algorithms must be well understood and respected.

The component based approach has the advantage of ease and flexibility in modeling variations of the vehicle; for some types of components such as lifting appendages there is a considerable body of archival data with which to build a model. But there are disadvantages: a component based model is inherently less accurate than one based on an extensive experimental database for the specific complete vehicle, although experience has shown that it can often give estimates within normal experimental error. The additional computational overhead of coordinate transformations also has to be considered.

Bohlmann used the component based approach to estimate manoeuvering coefficients that he then incorporated in a coefficient model [5]. The component model in DSSP50 avoids this intermediate step to gain flexibility, but at the expense of some computational complexity.

2.4 Coefficient Based Models

A coefficient model is implemented in DSSP50 using the concept of a lump. Lumps are handled as another kind of component but, as the name is meant to imply, there is no geometry associated with them. The hydrodynamic loads on a lump are obtained with a variant of the Gertler and Hagen (G&H) coefficient model [7].

The model attempts to represent the physics of the flow about the vehicle, including loads due to cross-coupling and nonlinearities. For example, a partial expansion of the normal force component of $\mathbf{F}(\mathbf{u})$ is:

$$\begin{aligned} Z(\mathbf{u}) \;=\; & \tfrac{1}{2}\rho\ell^4\left[Z'_{pp}p^2+\ldots\right]+\tfrac{1}{2}\rho\ell^3\left[Z'_{q}uq+\ldots\right]+ \\ & \tfrac{1}{2}\rho\ell^2\left[Z'_{*}u^2+Z'_{w}uw+Z'_{w|w|}w\left|\sqrt{v^2+w^2}\right|+Z'_{vv}v^2+\ldots\right] \end{aligned} \tag{10}$$

in which Z'_{pp}, etc., are the hydrodynamic coefficients. Each term in the equation corresponds to one or more physical load generating mechanisms. Thus, in the above equation $\frac{1}{2}\rho\ell^2 Z'_{w|w|}w\left|\sqrt{v^2+w^2}\right|$ is crossflow damping and $\frac{1}{2}\rho\ell^2 Z'_{vv}v^2$ is the out-of-plane normal force generated by a hull bound vortex. The six equations that make up the full coefficient model are given in section 7.

A lump can represent anything from a nonstandard component to the whole vehicle. Nonstandard components are those that are not well represented by the component model, such as a sonar fairing that introduces significant drag components or a slender wing that the low aspect ratio algorithms do not model. The only requirement is that the necessary coefficients are known or can be estimated with sufficient accuracy.

When a lump is used to model the hydrodynamics of the whole vehicle, the coefficients are typically derived from experiments with fully-outfitted models. Without knowing how the experiments were done, caution is required in interpreting the damping coefficients Z'_w, etc. In form they correspond to stability derivatives, but can only be so used if obtained at small angles of incidence. It is straightforward to obtain them by regression on a small-incidence subset of the experimental data (so long as it is sufficiently populated) and plug in those values to regress the other coefficients and parameters from the complete data set, but the resulting model may be overall less accurate than if all coefficients, including damping, are regressed simultaneously from the complete data set. In the latter case, the damping coefficients should be described as manoeuvering coefficients, and stability derivatives should be obtained separately.

Alone, coefficient based models lack flexibility for accommodating variations of the vehicle, making them of limited use for systematic series and design studies. Unless

parameter based coefficients derived for a set of similar vehicles are available, extensive physical testing may be needed to acquire the coefficient values for each variation.

2.5 DSSP50

DSSP50 combines the component and coefficient loads models described in the preceeding sections:

$$\mathbf{F}(\mathbf{u}) = \sum_i w_i \mathbf{C}_i(\mathbf{u}) + \sum_i \sum_{j,j \neq i} w_{i,j} \mathbf{C}_{i,j}(\mathbf{u}) + \sum_k w_k \mathbf{D}_k(\mathbf{u}) \tag{11}$$

where w_i etc. are weights and $\mathbf{D}_k$ are the lump (coefficient) contributions to the loads. There are $i = j$ hull and appendage components, and k lumps. When both component and coefficient models are present, the combination is called a hybrid model of the vehicle loads.

The weights are by default equal to one, in which case all the load contributions are simply added. However, the user may specify values of zero or minus one in order to ignore or subtract one or more contributions. A typical example of doing this would be to substitute a new set of rudders on a vehicle that is represented as a lump. So long as the basic geometry of the new and old rudders is known well enough, the old set can be subtracted and the new set added as appendage components. This procedure is illustrated in the tutorial in reference [1].

3 Axis Systems

The principal axis systems in DSSP50 are discussed in section 3.4 of the program guide [1] and sketched here in figure 1. It is usually easy to tell from the context which axis system is being used. Hydrodynamic calculations for individual components are, as previously noted, formulated in local axes; tail appendage local axes are shown on the figure. Most hydrodynamic and load output from the program is in boat-fixed reference axes. Exceptions are noted in the program guide. In a free manoeuver, velocities, rotational rates, and loads in the equations of motion are in reference axes, while trajectory and attitude are in earth-fixed inertial axes. Both systems are right handed; reference axes have x forward, y to starboard, and z downwards.

Vehicle axes also shown on figure 1 are used for defining the geometry of the vehicle and are not used in any of the discussions here.

4 Hull Component Loads

Hull loads can be divided into the in-plane loads, which occur in the same plane that incidence is measured, and the out-of-plane loads, which occur in the other plane because of some asymmetry. For example, in yaw the in-plane loads are Y and N and the

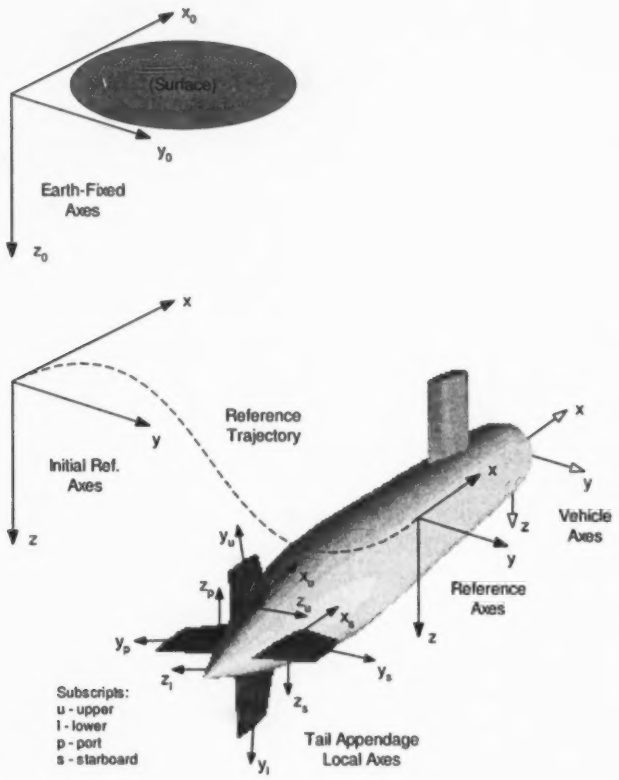

Figure 1. Principal earth-fixed and boat-fixed axis systems [1].

out-of-plane loads are Z and M. In DSSP50, only in-plane loads are associated directly with the hull, while out-of-plane loads are calculated separately.

In-plane loads are typically calculated from potential flow with viscous corrections. A summary of Munk's potential flow calculation and some methods of viscous correction is given in reference [8]; they apply to slender hulls with near-circular cross sections. The method originally adopted in the earlier code DSSP20 was Hooft's version, called HulFor [9].

4.1 HulFor Calculations

Expressed in terms of incidence angle or crossflow velocity, the potential flow contribution is identified with the linear component of the normal force distribution, and the

viscous contribution with a nonlinear component. In this simple model, the total hull normal force and pitching moment due to heave are expressed as:

$$\begin{aligned} Z &= \tfrac{1}{2}\rho\ell^2 \left[Z'_w uw + Z'_{w|w|} w|w| \right] \\ M &= \tfrac{1}{2}\rho\ell^3 \left[M'_w uw + M'_{w|w|} w|w| \right] \end{aligned} \tag{12}$$

The `HulFor` method calculates the linear terms of equations (12) with slender body theory, and the nonlinear terms using an empirical function for local crossflow drag. Loads due to rotation are calculated the same way. Because better results are obtained with the methods discussed below, using the `HulFor` method for translational loads is deprecated in the current build of `DSSP50`. However, it is still used for rotational loads since there is no available substitute.

4.2 Empirical Predictions

The `DSSP50` build 090910 default method of estimating in-plane hull loads is a revision of Ward and Lloyd's [10] empirical prediction of the coefficients in equations (12). In the revised model, coefficients regressed from a database of 32 axisymmetric hulls are interpolated with respect to prismatic coefficient C_P and slenderness ratio L/D using either Kriging interpolation or neural network generalization [8]. Little difference has been found in practice between the two methods. The results are formulated as two-dimensional lookup tables. Reynolds number (based on hull length) for tests in the experimental database is in the range 6.3 to 23 million, and the predictions are presumed to be valid over at least this range. There is at present very little guidance on how to scale these in-plane predictions up to full scale Reynolds numbers, or even whether it is necessary to do so.

4.3 Jeans Method

The Jeans method is founded on slender body theory and uses the viscous impulse method to model the effect of afterbody separation [11]. A universal expression for the axial distribution of the impulse was derived from experimental and CFD-generated data for a small subset of the database used in the regression model described above; the hulls ranged in L/D from 6 to 9. A practical implementation of the procedure is outlined in the appendix to reference [11].

In an unpublished study, the author did calculations for the full experimental database using the Jeans method as implemented in `DSSP50`. Agreement with results for the empirical method and with the data was generally reasonable although the method may tend to overpredict the longitudinal moment. Figure 44 from reference [8] with Jeans results added is shown here as figure 2. Note that the Albert model is not in the experimental database but was used for independent verification. The hull is not axisymmetric and even in pitch there may be effects of its keel and deck casing in the data.

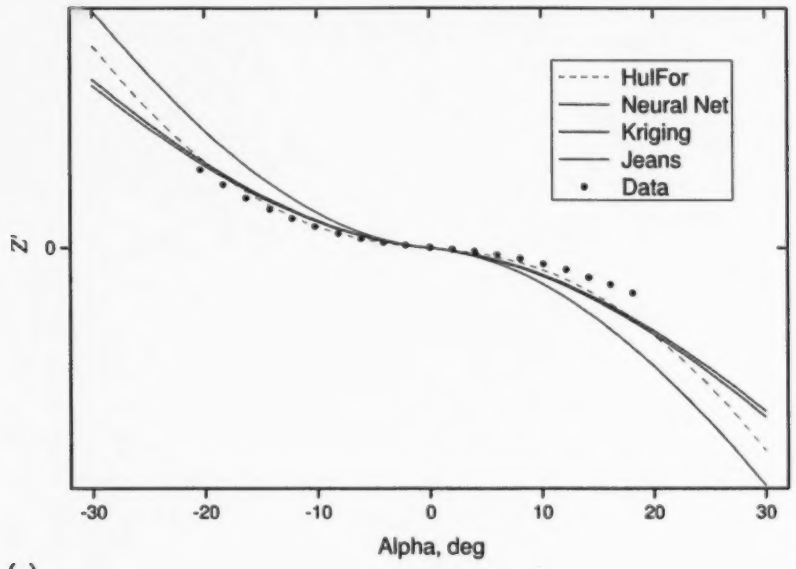

(a)

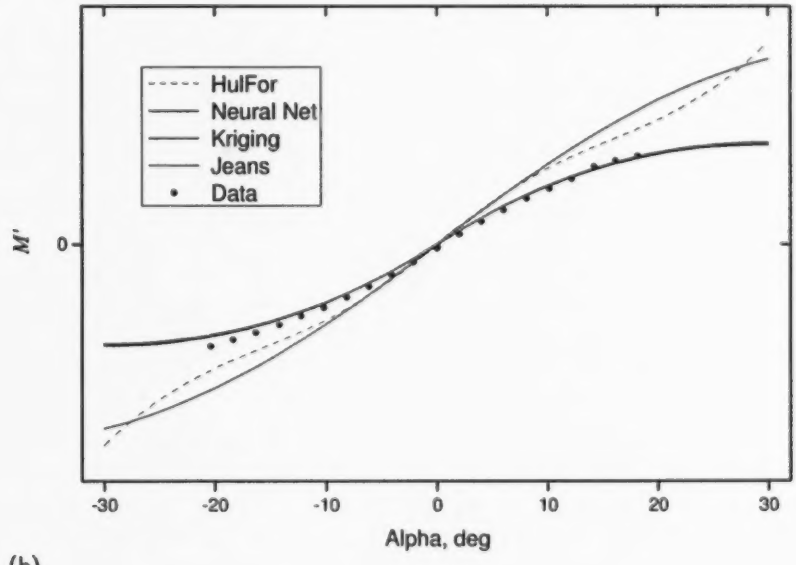

(b)

Figure 2. Comparison between in-plane load data and predictions for the Albert hull in pitch [8]: (a) Z' and (b) M'.

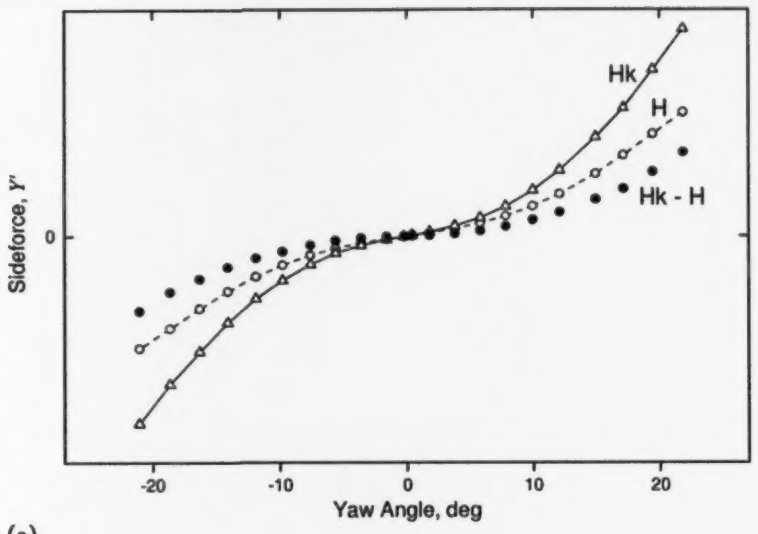

(a)

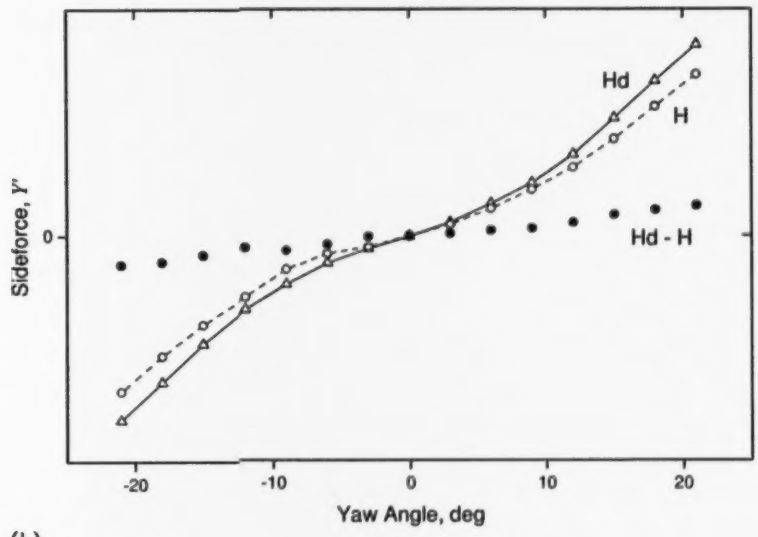

(b)

Figure 3. The effect of a keel and deck on sideforce [8]: (a) for the Albert hull and keel, Hk, and (b) for the Standard Model hull and deck, Hd. In each case, H is for the hull alone.

4.4 Keel and Deck

The presence of a keel or deck on an axisymmetric hull in yaw usually leads to a sideforce Y and yawing moment N that are significantly greater than can be explained by the corresponding increase in hull depth alone. This is illustrated for sideforce in figure 3. In `DSSP50`, corrections can be made for this increase using a `Keel` or `Deck` input record. The user guide suggests values for the increase but, if available, strip test data for a similar hull/keel/deck combination will likely provide a better estimate.

4.5 Hull Drag

The requirement for accuracy in estimating axial force for a free simulation is less stringent than for other loads since uncertainties in drag can be compensated for in the propulsion model. Drag, or axial force, prediction has therefore received less attention than have the transverse loads. A small incidence approximation of the axial load on a hull in pitch is outlined in reference [12], wherein:

$$X' = -D'_0 - \frac{1}{2} Z'_w w^2 \tag{13}$$

There is an equivalent expression for yaw. The zero-incidence drag D'_0 is given by:

$$D'_0 = \frac{\rho}{2} u^2 A_{wet} \left[C_F (1 + C_{\Delta f}) + k_r + \frac{0.029}{\sqrt{C_F}} \left(\frac{A_{base}}{A_{wet}} \right)^{\frac{1}{2}} \right] \tag{14}$$

where A_{wet} is hull wetted area; C_F is the friction drag coefficient, which uses the Schoenherr line for turbulent flow [13]; $C_{\Delta f}$ is the residual drag coefficient (input record `ResiDragR`); k_r is the roughness allowance coefficient (input record `RoughAllow`); and A_{base} is the base area for a truncated hull. The last term, base drag, is derived from Hoerner [14].

5 Appendage Component Loads

Lifting appendage loads were extensively reviewed in reference [15]. The estimation methods described therein, which with a few modifications are still used in `DSSP50`, are summarized below. A short summary of tailplane efficiency calculation, a newer development, follows.

5.1 Summary of Appendage Load Prediction

Appendage loads, which are calculated in local axes, are discussed here as coefficients C_Z and C_X, nondimensionalized by the appendage chord and span. The coefficients have been modified from Aucher's formulation of the loads on an isolated fin [16]:

$$C_Z = C_{Z\alpha}(\alpha_\bullet + \alpha_g) - 2.1\alpha^3_{\bullet(\alpha)} \tag{15}$$

$$\begin{aligned} C_X &= -0.01 + 0.7a_e\alpha^2_{\bullet(\alpha)} + C_{Z\alpha}\alpha^2_{\bullet(0)} - 2.1\alpha^4_{\bullet(0)} + \\ &\quad k_\delta\left(\frac{\overline{c_f}}{\overline{c}}\right)\left(\frac{b_2 - b_1}{b_{exp}}\right)|\delta|^{\frac{3}{2}} + C_{Xj}\left(\frac{t}{c}\right)^2\frac{\overline{c}^2}{S} \end{aligned} \tag{16}$$

The principal parameters in equations 15 and 16 are discussed in this section, and a complete list will be found in the nomenclature. The equations contain corrections to account for interference between the appendage and the hull it is mounted on. Most of these corrections have been combined into $\alpha_\bullet$, an augmented angle of incidence corresponding to the corrected total normal force generated by the appendage. This angle has two components: the first, subscripted by (α), is associated with geometric incidence; the second component, subscripted by (0), arises from lift due to a control deflection, roll, or pitch:

$$\alpha_\bullet = \alpha_{\bullet(\alpha)} + \alpha_{\bullet(0)} \tag{17}$$

where

$$\alpha_{\bullet(\alpha)} = \left[k_s\, k_{sp}\, K_{WB}\, f(\phi)\cos^2\phi\right]\alpha \tag{18}$$

and

$$\begin{aligned} \alpha_{\bullet(0)} &= \sqrt{k_s}\, K_{WB}\, f(\phi)\left[\frac{1}{\sqrt{k_s}}\frac{C_{Z\alpha(ep)}}{C_{Z\alpha}}\frac{k_{WB}}{K_{WB}}\tau\,\eta\,\sigma\,\delta_e + J\,p' + \right. \\ &\quad \left.\left(a_e J\tan\Omega_{c/2} + \left(1 + \frac{1}{4a_e}\right)\frac{\cos^2\phi}{2}\right)q'\right] \end{aligned} \tag{19}$$

Geometric camber f and twist α_b are combined into a zero-incidence equivalent angle α_g [17]:

$$\alpha_g = -\left(1 + \frac{1}{4a_e}\right)2f + J\,\alpha_b \tag{20}$$

The basic normal force slope is as given by Aucher [16]:

$$C_{Z\alpha} = \frac{-2\pi a_e\left[1 - 3\left(\frac{t}{c}\right)^2\right]}{2.6 + \cos\Omega\sqrt{2 + \frac{a_e^2}{\cos^2\Omega}}} \tag{21}$$

Many of the quantities in this section depend on the geometrical quantities sketched in figures 4 to 6. For example, the effective aspect ratio a_e incorporates endplate corrections k_{ep} and k'_{ep} [18,19]:

$$a_e = \frac{2b}{\overline{c}} \left[1 + (k_{ep} - 1) \left(\frac{b_{ep}}{b} \right)^2 \right] k'_{ep} \tag{22}$$

Other parameters in equations (15) to (22) are defined as follows:

- b is appendage semispan measured from the hull centerline or a similar datum: $b = b_{exp} + (1/b_{exp} + 1/r)^{-1}$ for a sail or a small bowplane not too far forward on the nose, b is equal to half this value for a ship stabilizer, b is measured from appendage tip to hull axis for a sternplane, rudder, or large bowplane, and b is measured from tip to the sail centerline for a sailplane.
- C_{Xj} is the junction axial force coefficient, typically depending on t/c [14]. If it is required, a value must be provided on the `CXJ` input record.
- $C_{Z\alpha(ep)}$ is the normal force slope calculated with no endplate correction for a flapped appendage, but including the correction for an all-moving appendage. In the latter case, the ratio $C_{Z\alpha(ep)}/C_{Z\alpha}$ is always equal to unity.

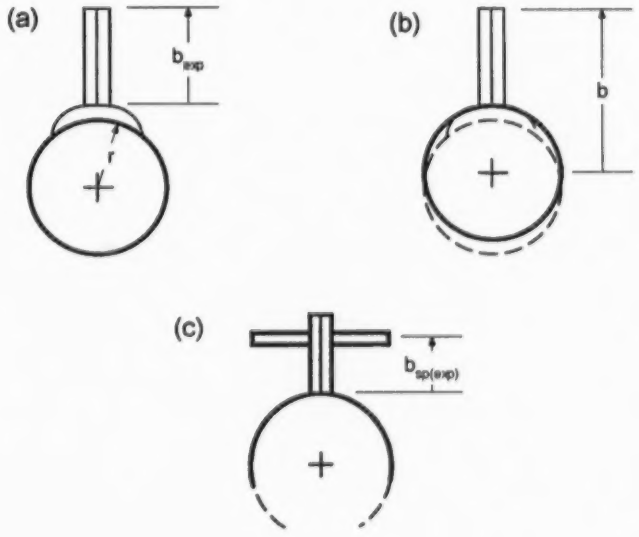

Figure 4. Hull/sail parameter nomenclature: (a) non-axisymmetric hull, (b) equivalent axisymmetric hull, and (c) sailplane location.

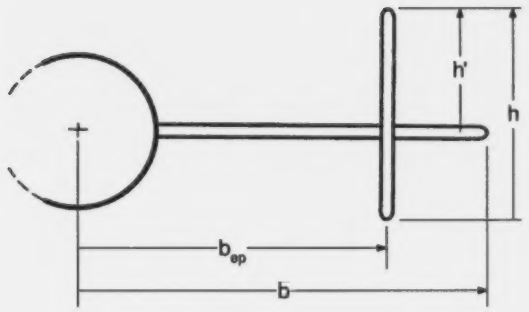

Figure 5. Endplate parameter nomenclature.

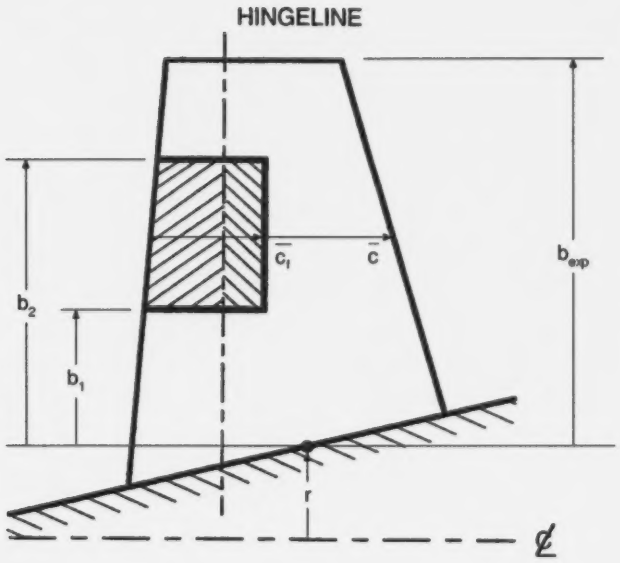

Figure 6. Flapped appendage parameter nomenclature.

- J, which is equal to about 0.4, is the ratio of lift slopes due to roll and to incidence. The following is an approximation to numerical experiments reported by Abbott and von Doenhoff [20]:

$$J \equiv \frac{C_{Z\gamma'}}{C_{Z\alpha}} = 0.4 + (\lambda - 0.5)\left(0.0125 a_e - 0.00035 a_e^2\right) \tag{23}$$

- k_{ep} is a parameter for an appendage with an endplate; it is given by [18]:

$$k_{ep} = 1 + 1.9\frac{h}{2b} - 0.5\left(\frac{h}{2b}\right)^2 \quad \text{for} \quad \frac{h}{b} \leq 2.5 \tag{24}$$

For other appendages k_{ep} is equal to unity.

- k'_{ep} is a parameter for an appendage that is itself an endplate [19]; it can be approximated by:

$$k'_{ep} = 1 + 2\left(\frac{h'}{h} - 0.5\right)^2 \tag{25}$$

For other appendages k'_{ep} is equal to unity.

- Sail efficiency $k_s = (1 + b_{de}/b_e)^2$ for a submarine sail [6,15], where b_{de} and b_e are illustrated in figure 7, and b_e is measured from tip to hull axis. The same correction is applied to a small bowplane so long as it is not too near the nose, using $b_{de} = r$; otherwise k_s is equal to unity.

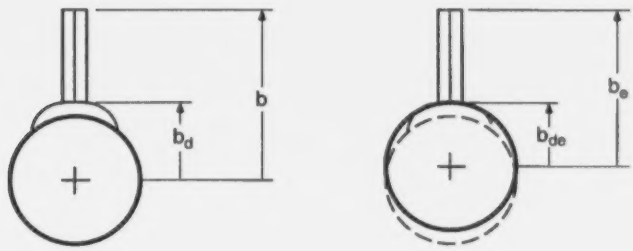

Figure 7. Sail and deck casing parameter nomenclature.

- Sailplane efficiency k_{sp} is given by [21]:

$$k_{sp} = 1 - \left(\frac{b_d}{b_{sp}}\right)^2 \tag{26}$$

For other appendages it is equal to unity. Deck height b_d and sailplane location b_{sp} are shown in figure 8; if there is a deck casing, modified parameters analogous to those on the right hand side of figure 7 are more appropriate.

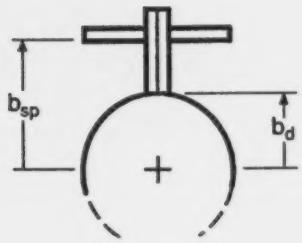

Figure 8. Sailplane parameter nomenclature.

- k_δ is the flap profile axial force coefficient; it may be defined on the `FlaProDrag` input record.
- K_{WB} and k_{WB} are the tailplane efficiencies for incidence and control deflection, respectively [22]. Their estimation is outlined in section 5.2.
- δ_e is effective flap angle. Unless the `DelNonLin` input record is present, $\delta_e = \delta$. With `DelNonLin`, an empirical correction is made for flap separation:

$$\delta_e = \begin{cases} \delta\,(1 - 1.6725\,\delta^2 + 1.1125\,\delta^3) & \text{for} \quad 0 \le \delta < 0.575 \\ 0.37865 + 0.19658(\delta - 0.575) & \text{for} \quad 0.575 \le \delta < 1.05 \end{cases} \tag{27}$$

  `DelNonLin` should not be used for all-moving control appendages. The above is a rough approximation based on a limited number of data; its accuracy is estimated to be within ±15 percent [15].

- η is a correction for flap balance and gap efficiency. If it is required, a value must be provided on the `FlapGap` input record.
- Spanwise flap efficiency σ is equal to $\sigma_2 - \sigma_1$ where σ_i is given by

$$\sigma_i = (1.6 - 0.32\lambda)\frac{b_i}{b_{exp}} - (0.6 - 0.32\lambda)\left(\frac{b_i}{b_{exp}}\right)^2 \qquad i = 1, 2 \tag{28}$$

  for a flap (figure 6), or σ is simply the moving/total area ratio:

$$\sigma = \frac{S_m}{S_{exp}} \tag{29}$$

  for an all-moving appendage [15].

- Chordwise flap efficiency τ is given by

$$\tau = 0.735\sqrt{\frac{c_f}{c}} + 0.647\frac{c_f}{c} \tag{30}$$

for a flap and is equal to unity for an all-moving appendage [15].

- ϕ is the local dihedral or anhedral angle for small bowplanes, and is zero otherwise; $f(\phi)$ is Nonweiler's dihedral factor [23], which can be approximated by:

$$f(\phi) \equiv f\left(k\frac{\pi}{2}\right) = 1 - 1.8k^2 + 0.8\,|k|^3 \tag{31}$$

where $k = \phi/(\pi/2)$.

As noted, many of the parameters discussed above depend on appendage type or control type. To use equations (15) to (22) for all appendages, inappropriate parameters are assigned a value, zero or one, to negate their effect. This is summarized in table 1, below.

Table 1. Appendage load parameter dependence (indicated by a check, √) or assigned value by (a) appendage and (b) control type.

(a)

Appendage Type	k_s	k_{sp}	K_{WB}	k_{WB}	ϕ	$f(\phi)$
`LBowplane`	1	1	1	1	0	1
`Rudder`	1	1	√	√	0	1
`Sail`	√	1	1	1	0	1
`Sailplane`	1	√	1	1	0	1
`SBowplane`	√	1	1	1	√	√
`Sternplane`	1	1	√	√	0	1
`Tail`	1	1	√	√	0	1

(b)

Control Type	K_{WB}	k_{WB}	η	σ	τ
`AllMoving`	√	√	1	√	√
`Flapped`	√	√	√	√	√

To calculate dimensional loads, the appropriate reference area is:

- for a sail or small bowplanes, the exposed appendage area S_{exp};
- for sternplanes, rudders, or large bowplanes, the augmented area produced by projecting the root chord to the hull axis; and
- for sailplanes, the augmented area produced by projecting the root chord to the sail centerline.

Moments on the appendage are calculated by assuming that the various components of Equations (15) and (16) act at the center of pressure given by a spanwise location, approximated by assuming elliptical loading:

$$C_{Pb} = \frac{4}{3\pi} \tag{32}$$

and a chordwise location, which from estimates in Aucher [16] is:

$$C_{Pc} = 0.05 + 0.1\sqrt{a_e} \quad \text{for} \quad a_e < 3 \tag{33}$$

Modifications to the center of pressure for lift due to twist and camber are discussed in reference [15]. Where there is lift carry-over, equation (32) is applied from the hull centerline.

5.2 Tailplane Efficiency

In some predecessors of this program, tailplane efficiency due to a control deflection, k_{WB}, was not distinguished from that due to incidence, K_{WB}; in reference [15] the symbol $k_{\eta t}$ is used for both. Efficiency $k_{\eta t}$ was estimated semiempirically from Dempsey's [24] or Lyons and Bisgood's [19] results according to Reynolds number. This approach has been discarded, and the current calculation is based on Bohlmann's modified Spreiter Method [22,25].

In this method, efficiency coefficients are derived for an equivalent triangular wing. The incremental normal force, Z_{WB} (that for the wing-body configuration less that for the body alone) comprises two components: $Z_{W(B)}$, force on the wing in the presence of the body, and force on the body arising from the presence of the wing. In relation to the force on an equivalent isolated appendage, Z_W, the efficiencies are:

$$K_{WB} = \int_0^1 \frac{d}{d\xi}\left(\frac{dZ_{WB}}{dZ_W}\right)_{\alpha=0} d\xi \tag{34}$$

and

$$k_{WB} = \int_0^1 \frac{d}{d\xi}\left(\frac{dZ_{W(B)}}{dZ_W}\right)_{\delta=0} d\xi \tag{35}$$

where

$$\frac{d}{d\xi}\left(\frac{dZ_{WB}}{dZ_W}\right)_{\alpha=0} = -2\frac{\sigma c_1}{b^2}\left[\frac{d\sigma}{d\xi}\left(1-\left(\frac{r}{\sigma}\right)^4\right) + 2\frac{dr}{d\xi}\left(\frac{r}{\sigma}\right)^3 + \frac{1}{\pi}\frac{dr}{d\xi}\left[1-\left(\frac{r}{\sigma}\right)^2 - \frac{\left(1+\left(\frac{r}{\sigma}\right)^2\right)^2}{2\left(\frac{r}{\sigma}\right)}\sin^{-1}\left(\frac{2\left(\frac{r}{\sigma}\right)}{1+\left(\frac{r}{\sigma}\right)^2}\right)\right]\right] + 2\frac{rc_1}{b^2}\frac{dr}{d\xi} \tag{36}$$

and

$$\frac{d}{d\xi}\left(\frac{dZ_{W(B)}}{dZ_W}\right)_{\delta=0} = -2\frac{\sigma c_1}{b^2}\left[\frac{d\sigma}{d\xi}\left(1-\left(\frac{r}{\sigma}\right)^4\right)+2\frac{dr}{d\xi}\left(\frac{r}{\sigma}\right)^3+\right. \tag{37}$$

$$\left.\frac{1}{\pi}\left[-2\frac{dr}{d\xi}\left(1+\left(\frac{r}{\sigma}\right)^2\right)\left(\frac{r}{\sigma}\right)-\right.\right.$$

$$\left.\left.\frac{d\sigma}{d\xi}\left(1-\left(\frac{r}{\sigma}\right)^4\right)\right]\sin^{-1}\left(\frac{2\left(\frac{r}{\sigma}\right)}{1+\left(\frac{r}{\sigma}\right)^2}\right)\right]$$

Geometrical quantities in the above equations are illustrated in figure 9; ξ is nondimensionalized by c_1.

For viscous flow, the hull radii and tail cone angle γ are adjusted by adding the local boundary layer displacement thickness δ^* to the hull. DSSP50 estimates δ^* from potential flow and thin turbulent boundary layer calculations [26,27] for an equivalent body-of-rotation hull in axial flow.

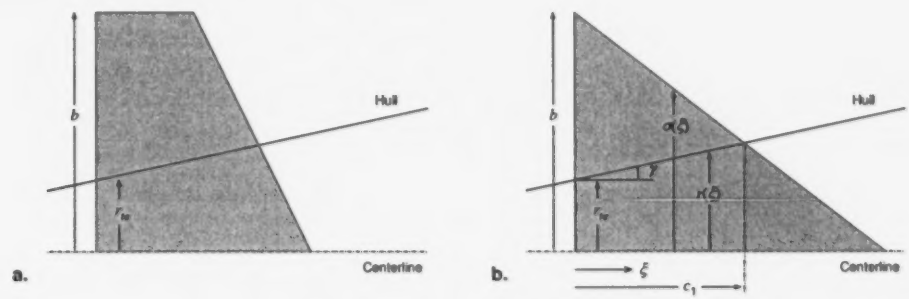

Figure 9. Geometry for the Bohlmann-Spreiter Method [22]: (a) a trapezoidal fin extended to the hull centerline and (b) its triangular equivalent. Dimensions b and r_{te} are the same, and the shaded regions have the same aspect ratio.

Experimental data show that the incremental normal force Z_{WB} can be characterized by two regions: an inner region with relatively low slope, and a fairly linear outer region with higher slope, figure 10. Values of tail efficiency predicted by the Bohlmann-Spreiter method generally correspond well with the outer slope, while cited values are frequently based on the inner slope. In any case, both are needed for a complete description of tail loads.

An empirical approximation to R, the ratio of the inner slope to the outer slope, is:

$$R = 0.65 + 0.35 f_1(\delta^*) - 0.45(1 - f_2(\gamma)) \tag{38}$$

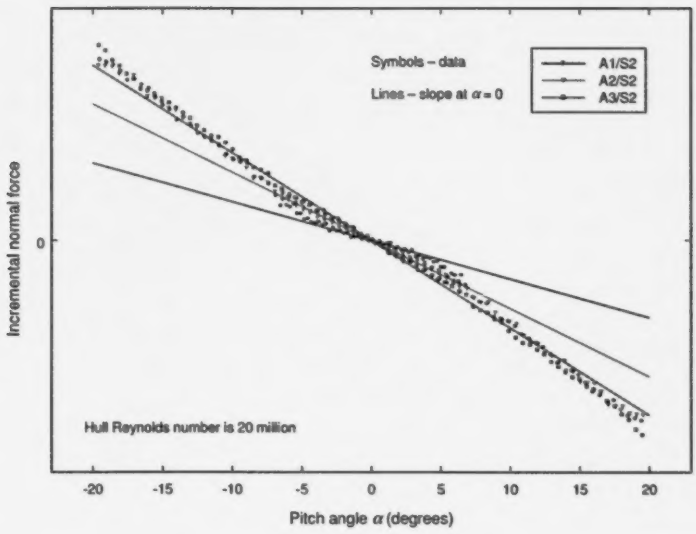

Figure 10. Incremental normal force *vs* pitch angle for three hull-appendage configurations: A1/S2, A2/S2, and A3/S2 [22], representing the same rudders on hulls with a tail-cone angle of 24.0, 18.5 and 14.0 degrees, respectively.

where f_1 and f_2 are sigmoid functions:

$$f_1(\delta^*) = \frac{1}{1 + e^{-\left(3 - 200\frac{\delta^*}{b}\right)}} \tag{39}$$

$$f_2(\gamma) = \frac{1}{1 + e^{-110(0.34 - \gamma)}} \tag{40}$$

The form of matching between inner and outer slopes was suggested by Watt, DRDC, in a private communication. In DSSP50 it is incorporated into an overall factor F, which multiplies the Bohlmann-Spreiter tailplane efficiency coefficients:

$$F(\alpha, \delta^*, \gamma) = 1 - (1 - R)e^{-\frac{200}{3}\alpha^2} \tag{41}$$

That is, tailplane efficiency over the whole range of incidence is given by:

$$\begin{aligned} K_{WB} &= F(\alpha, \delta^*, \gamma)\, K_{WB} \\ k_{WB} &= F(\alpha, \delta^*, \gamma)\, k_{WB} \end{aligned} \tag{42}$$

where the values on the right hand side are given by equations (34) to (37).

The procedure described above is the default in the program. Through the `TailEff` input record, a user may alternatively select Dempsey's method [24] for K_{WB} and apply

the inviscid Bohlmann-Spreiter efficiency ratio k_{WB}/K_{WB} to get k_{WB}, or input specific values of the coefficients. The coefficients are not subsequently corrected for incidence in either case. Comparison with some model data indicates the default calculation giving low efficiencies for all-moving control appendages; if this is suspected, selecting Dempsey's method is suggested.

6 Out-of-Plane Loads

`DSSP50` calculates the out-of-plane loads, which act on a hull due to the presence of (generally) a sail, separately from the hull and appendage loads discussed so far. This is automatic, requiring no user input, for appendages of type `Sail` so long as there is at least one hull. In addition, the user can invoke the calculation for any valid appendage/hull combination using `OOPCalc` input.

Circulation convected from a sail at incidence is bound to the hull (as well as shed from the tip), and with crossflow on the hull gives rise to a normal force distribution $\widehat{Z}$ on the hull aft of the sail according to the Kutta-Joukowski Theorem [28]. Physical and numerical experiments have shown that the bound circulation is distributed linearly, or nearly linearly, between being equal to the sail circulation at the sail trailing edge to zero at the tail. Since the local value of $\widehat{Z}$ is proportional to the local hull bound circulation, it, too, is nearly linear. In reference [28] it is shown that for a submarine in yaw the nondimensional loads can be estimated by:

$$Z' = \int_{x'_{AP}}^{x'_{TE}} \widehat{Z}'(x')dx' \quad \text{and} \quad M' = -\int_{x'_{AP}}^{x'_{TE}} x'\widehat{Z}'(x')dx' \tag{43}$$

where

$$\widehat{Z}'(x') = \frac{-v'(x')f(x')Y'_{sail}}{b'_e} \tag{44}$$

Y'_{sail} is sideforce on the sail and subscripts AP and TE refer to the aft perpendicular and the trailing edge of the sail, respectively; $f(x')$ is a nondimensional load distribution function. Since Y'_{sail} and the local crossflow velocity $v'(x')$ can be functions of time, this equation applies to both steady and unsteady flows. In unsteady flow, the instantaneous value of Y'_{sail} is convected aft at the current axial velocity.

The distribution function $f(x')$ is a modified ramp:

$$\begin{aligned} f(x') &= 1 && x' \geq x'_1 \\ &= \left[\frac{x' - x'_2}{x'_1 - x'_2}\right]^{m(\beta_c)} && x'_1 > x' > x'_2 \\ &= 0 && x'_2 \geq x' \end{aligned} \tag{45}$$

in which x'_1 and x'_2 define the ends of the ramp, and $m(\beta_c)$, where β_c is some critical drift angle, modifies the form of the distribution. For pure drift, $\beta_c = \beta$. If $m = 1$ the load distribution is linear. A simple way to represent the influence of drift angle is to use $m = 1 + k\beta_c$, where k is a constant. By default, $x'_1 = x'_{TE}$ and $x'_2 = x'_{AP}$.

A number of examples are shown in reference [28] for which, to match experimental loads, m varies from $1+3\beta$ (with β in radians) to $1-2\beta$. In some cases it was not possible to match both the force and moment well with the same value of k. However, in the absence of specific information on the out-of-plane characteristics, a linear distribution ($k = 0$, or $m = 1$) should be satisfactory for a preliminary estimate. This is the current default in the program.

7 Lump Loads

The full coefficient model for lump loads inherited from DSSP40 is as follows.

Axial force X:

$$\begin{aligned} X \;=\; & \tfrac{1}{2}\rho\ell^4\left[X'_{qq}q^2 + X'_{rp}rp + X'_{rr}r^2\right] + \tfrac{1}{2}\rho\ell^3\left[X'_{vr}vr + X'_{wq}wq\right] + \\ & \tfrac{1}{2}\rho\ell^2\left[X'_{*}u^2 + \left(X'_{vv} + k_nX'_{vvn}\right)v^2 + \left(X'_{ww} + k_nX'_{wwn}\right)w^2\right] + \\ & \tfrac{1}{2}\rho\ell^2\left[\left(X'_{\delta r\delta r} + k_nX'_{\delta r\delta rn}\right)u^2\delta_r^2 + \left(X'_{\delta s\delta s} + k_nX'_{\delta s\delta sn}\right)u^2\delta_s^2 + \right. \\ & \left. X'_{\delta b\delta b}u^2\delta_b^2\right] \end{aligned} \tag{46}$$

Sideforce Y:

$$\begin{aligned} Y \;=\; & \tfrac{1}{2}\rho\ell^4\left[Y'_{p|p|}p|p| + Y'_{pq}pq + Y'_{qr}qr\right] + \\ & \tfrac{1}{2}\rho\ell^3\left[Y'_{p}up + \left(Y'_{r} + k_nY'_{rn}\right)ur + Y'_{vq}vq + Y'_{wp}wp + \right. \\ & \left. Y'_{wr}wr + Y'_{v|r|}\frac{v}{|v|}\left|\sqrt{v^2+w^2}\right||r| + Y'_{|r|\delta r}u|r|\delta_r\right] + \\ & \tfrac{1}{2}\rho\ell^2\left[Y'_{*}u^2 + \left(Y'_{v} + k_nY'_{vn}\right)uv + \left(Y'_{v|v|} + k_nY'_{v|v|n}\right)v\left|\sqrt{v^2+w^2}\right| + \right. \\ & \left. Y'_{vw}vw + \left(Y'_{\delta r} + k_nY'_{\delta rn}\right)u^2\delta_r + Y'_{\delta s}u^2\delta_s + Y'_{\delta b}u^2\delta_b\right] \end{aligned} \tag{47}$$

Normal force Z:

$$\begin{aligned} Z \;=\; & \tfrac{1}{2}\rho\ell^4\left[Z'_{pp}p^2 + Z'_{rp}rp + Z'_{rr}r^2\right] + \\ & \tfrac{1}{2}\rho\ell^3\left[\left(Z'_{q} + k_nZ'_{qn}\right)uq + Z'_{vp}vp + Z'_{vr}vr + \right. \\ & \left. Z'_{w|q|}\frac{w}{|w|}\left|\sqrt{v^2+w^2}\right||q| + Z'_{|q|\delta s}u|q|\delta_s\right] + \\ & \tfrac{1}{2}\rho\ell^2\left[Z'_{*}u^2 + \left(Z'_{w} + k_nZ'_{wn}\right)uw + Z'_{vv}v^2 + Z'_{|w|}u|w| + \right. \\ & \left(Z'_{w|w|} + k_nZ'_{w|w|n}\right)w\left|\sqrt{v^2+w^2}\right| + Z'_{ww}\left|w\sqrt{v^2+w^2}\right| + \\ & \left. \left(Z'_{\delta s} + k_nZ'_{\delta sn}\right)u^2\delta_s + Z'_{\delta b}u^2\delta_b\right] \end{aligned} \tag{48}$$

Rolling moment K:

$$\begin{aligned} K \;=\; & \tfrac{1}{2}\rho\ell^5\left[K'_{p|p|}p|p| + K'_{pq}pq + K'_{qr}qr\right] + \\ & \tfrac{1}{2}\rho\ell^4\left[K'_{up}up + K'_{ur}ur + K'_{vq}vq + K'_{wp}wp + K'_{wr}wr\right] + \\ & \tfrac{1}{2}\rho\ell^3\left[\left(K'_{*} + k_n K'_{*n}\right)u^2 + K'_{uv}uv + K'_{v|v|}v\left|\sqrt{v^2+w^2}\right| + K'_{vw}vw + \right. \\ & \left. \left(K'_{\delta r} + k_n K'_{\delta rn}\right)u^2\delta_r + \left(K'_{\delta s} + k_n K'_{\delta sn}\right)u^2\delta_s + K'_{\delta b}u^2\delta_b\right] \end{aligned} \tag{49}$$

Pitching moment M:

$$\begin{aligned} M \;=\; & \tfrac{1}{2}\rho\ell^5\left[M'_{pp}p^2 + M'_{pr}pr + M'_{rr}r^2 + M'_{q|q|}q|q|\right] + \\ & \tfrac{1}{2}\rho\ell^4\left[\left(M'_{q} + k_n M'_{qn}\right)uq + M'_{vp}vp + M'_{vr}vr + \right. \\ & \left. M'_{|w|q}\left|\sqrt{v^2+w^2}\right|q + M'_{|q|\delta s}u|q|\delta_s\right] + \\ & \tfrac{1}{2}\rho\ell^3\left[M'_{*}u^2 + \left(M'_{w} + k_n M'_{wn}\right)uw + M'_{vv}v^2 + M'_{|w|}u|w| + \right. \\ & \left(M'_{w|w|} + k_n M'_{w|w|n}\right)w\left|\sqrt{v^2+w^2}\right| + M'_{ww}\left|w\sqrt{v^2+w^2}\right| + \\ & \left(M'_{\delta r\delta r} + k_n M'_{\delta r\delta rn}\right)u^2\delta_r\delta_r + \left(M'_{\delta s} + k_n M'_{\delta sn}\right)u^2\delta_s + \\ & \left. M'_{\delta b}u^2\delta_b\right] \end{aligned} \tag{50}$$

Yawing moment N:

$$\begin{aligned} N \;=\; & \tfrac{1}{2}\rho\ell^5\left[N'_{pq}pq + N'_{qr}qr + N'_{r|r|}r|r|\right] + \\ & \tfrac{1}{2}\rho\ell^4\left[N'_{up}up + \left(N'_{r} + k_n N'_{rn}\right)ur + N'_{wp}wp + N'_{wr}wr + N'_{vq}vq + \right. \\ & \left. N'_{|v|r}\left|\sqrt{v^2+w^2}\right|r + N'_{|r|\delta r}u|r|\delta_r\right] + \\ & \tfrac{1}{2}\rho\ell^3\left[N'_{*}u^2 + \left(N'_{v} + k_n N'_{vn}\right)uv + \left(N'_{v|v|} + k_n N'_{v|v|n}\right)v\left|\sqrt{v^2+w^2}\right| + \right. \\ & N'_{vw}vw + \left(N'_{\delta r} + k_n N'_{\delta rn}\right)u^2\delta_r + \left(N'_{\delta s\delta s} + k_n N'_{\delta s\delta sn}\right)u^2\delta_s\delta_s + \\ & \left. N'_{\delta b\delta b}u^2\delta_b\delta_b\right] \end{aligned} \tag{51}$$

In these equations, k_n represents the propulsion state:

$$\begin{aligned} k_n \;&=\; -2 && n' < -1 \\ &=\; n' - 1 && \text{otherwise} \end{aligned} \tag{52}$$

where n' is the ratio of actual RPM to self-propulsion RPM. This formulation is generally used to capture the effects of a large single propulsor on the aft hull and stern appendages. However, in the program it can be used for other arrangements, and if n' is different for different propulsors, the mean value is used.

The model includes a small number of terms, not found in G&H, that do not apply to most submarines. For example, the term associated with $N'_{\delta b\delta b}$ implies an asymmetric bowplane arrangement.

Length ℓ used in nondimensionalizing the coefficients is normally, and by default, the hull length of the vehicle. (If a hull component is not specified, ℓ has to be provided.) Coefficients from some sources may be nondimensionalized with an area and a length (i.e., for wings, planform area and span), in which case their values will have to be scaled so that the area is equal to ℓ^2.

8 Propulsion

Propulsion is only used in a free-swimming vehicle simulation. The basic function of the propulsion model is to provide propulsor thrust and torque coefficients, K_T and K_Q, at a given RPM and boat speed.

$$\begin{aligned} K_T &= \frac{T}{\rho n^2 D_P^4} \\ K_Q &= \frac{Q}{\rho n^2 D_P^5} \end{aligned} \tag{53}$$

where n is propulsor revolutions per second (although here, as in other references, the shaft rate is often loosely referred to as the RPM), D_P is propulsor diameter, T is thrust, and Q is torque.

The default propulsion model in `DSSP50` was suggested by J.L. Kennedy, DRDC, in a private communication. It derives the coefficients from Wageningen B4–70 propeller series data [29], and in the absence of a user-supplied value attempts to optimize the pitch/diameter ratio for maximum efficiency. In practice this ratio is generally at the low end of the range, about 0.6. Reynolds number effects, as discussed in reference [29], have not been modeled. The effect of propeller pitch/diameter ratio is illustrated in figure 11; the coefficient definitions used in the figure are in terms of the hydrodynamic pitch angle $\beta = \tan^{-1}[U/(0.7\pi n D_P)]$:

$$\begin{aligned} C_T^* &= \frac{T}{\frac{1}{2}\rho [U \csc\beta]^2 \frac{\pi}{4} D_P^2} \\ C_Q^* &= \frac{Q}{\frac{1}{2}\rho [U \csc\beta]^2 \frac{\pi}{4} D_P^3} \end{aligned} \tag{54}$$

`DSSP50` interpolates over lookup tables of these data and converts the results to open water K_T and K_Q coefficients. Behind-the-hull values are obtained with empirical estimates of the wake fraction and thrust deduction attributed to Barr in reference [30].

Uncorrected open water Wageningen B coefficients can be selected with the `Open` input record. This may be appropriate for propellers in the old twin-screw arrangement, but a better choice in that case might be to use the `DSSPtwo` propulsion model, which is modified from the Oberon class `DSSP02` code [31].

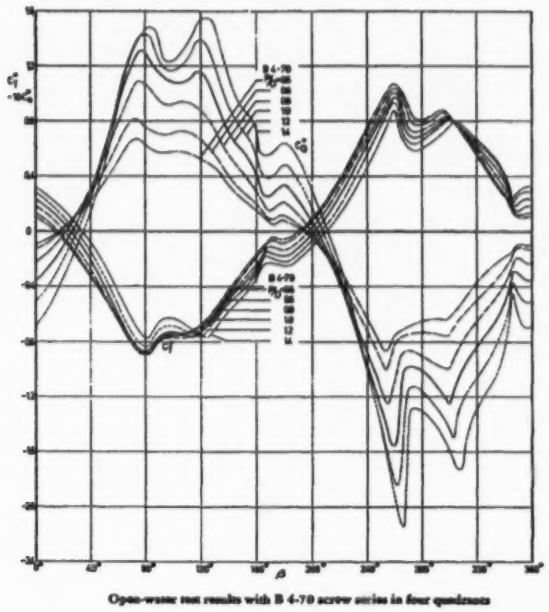

Figure 11. The effect of pitch/diameter ratio on Wageningen B4–70 propeller series data [29].

RPM remains constant unless it is different from the commanded value n_c, in which case propulsor revolutions are governed by the second order linear differential equation:

$$\ddot{n} + 2\zeta_n \omega_n \dot{n} + \omega_n^2 n \;=\; \omega_n^2 n_c \tag{55}$$

Damping ζ_n and response frequency ω_n are defined with a `RevDynam` input record. The magnitude of $\dot{n}$ is clipped at $\pm \dot{n}_M$, which is set by a `RevRateLim` input record. In this model, RPM is determined only by n_c, not by the load on the propulsor. Alternatively, the system will approximate constant power, speed, or thrust modes using the propulsion autopilot, which is activated with an `AutoProp` input record. In these modes the current value of n_c is generated by the autopilot.

For integration in time, equation (55) is decomposed into two first order equations:

$$\begin{aligned} \frac{d}{dt} n &= \dot{n} \\ \frac{d}{dt} \dot{n} &= -2\zeta_n \omega_n \dot{n} + \omega_n^2 (n_c - n) \end{aligned} \tag{56}$$

Here and elsewhere, d/dt is used in an equation to be integrated in a free manoeuver, otherwise dot notation is used to indicate time derivatives.

An aspect of electric propulsion systems is that the RPM range may not be continuous but composed of a series of groups, each requiring different external resistances to keep the motor armature and field currents within specifications. The result of having to switch resistances when changing RPM is that its time history is somewhat irregular. In `DSSP50` the user can specify a short time delay between groups during which n is constant. This is not supposed to model the actual RPM time history but to provide a representative delay, due to group switching, in the time taken to change n.

A `RevGroups` record in *Root*`.geo` is required to set up propulsion groups [2]. By default there are no groups, and RPM changes are continuous.

9 Control Deflection Dynamics

Control deflections are calculated for appendage components defined as controls, and for lumps with nonzero control coefficients. Like propulsor RPM, the deflections, δ, are governed by a second order linear differential equation:

$$\ddot{\delta} + 2\zeta_\delta \omega_\delta \dot{\delta} + \omega_\delta^2 \delta \;=\; \omega_\delta^2 \delta_c \tag{57}$$

Damping ζ_δ and response frequency ω_δ are defined with a `DeltaDyn` input record for appendages. The magnitude of $\dot{\delta}$ is clipped at $\pm\dot{\delta}_M$, which is set by a `DelRateLim` input record. There are equivalent inputs for lumps.

Actual and commanded deflections are monitored independently for each appendage and lump in local axes. Syntax described in the input reference allows a user to set values of δ_c for multiple controls with a simple command. Values of δ_c are also generated by the depth, heading, and roll autopilots, if activated.

For integration in time, equation (57) is decomposed into two first order equations:

$$\begin{aligned} \frac{d}{dt}\delta &= \dot{\delta} \\ \frac{d}{dt}\dot{\delta} &= -2\zeta_\delta \omega_\delta \dot{\delta} + \omega_\delta^2 (\delta_c - \delta) \end{aligned} \tag{58}$$

10 Autopilots

`DSSP50` autopilot algorithms are discussed in references [1] and [2]. Error signals for the autopilots are as follows. For depth:

$$J_{E\,(\text{depth})} = \left[\left[z_{0c} - z_0 \right]_{-l_z \sin\theta_L}^{+l_z \sin\theta_L} \;+\; l_z \sin\theta \right] C_{E\,(\text{depth})} \tag{59}$$

for heading:

$$J_{E\,(\text{heading})} = [\psi_c - \psi]\, C_{E\,(\text{heading})} \tag{60}$$

for propulsion, according to whether the control parameter is power, speed, or thrust:

$$\begin{aligned} J_{E\,(\text{prop})} &= \left[P_c^{1/3} - P^{1/3}\right] C_{E\,(\text{prop-power})} \qquad \text{or} \\ &= [u_c - u]\, C_{E\,(\text{prop-speed})} \qquad \text{or} \\ &= \left[T_c^{1/2} - T^{1/2}\right] C_{E\,(\text{prop-thrust})} \end{aligned} \tag{61}$$

and for roll:

$$J_{E\,(\text{roll})} = [\phi_c - \phi]\, C_{E\,(\text{roll})} \tag{62}$$

In equations (59) to (62), subscript nomenclature is as in the input reference. Error signals are clipped at ± 1.

The phase lead method used for deriving a corresponding control signal J_C is formulated in DSSP50 as:

$$\dot{J}_C = \frac{\alpha}{\tau}\left[J_E + \tau \dot{J}_E - J_C\right] \tag{63}$$

where α and τ are a characteristic gain and time constant respectively. For integration in time this is rearranged in terms of $J_C - \alpha J_E$:

$$\frac{d}{dt}(J_C - \alpha J_E) = -\frac{\alpha}{\tau}\left[(J_C - \alpha J_E) + (\alpha - 1) J_E\right] \tag{64}$$

The alternative method of deriving J_C uses a PID formulation:

$$J_C = K_P\, J_E + K_I \int J_E\, dt + K_D\, \dot{J}_E \tag{65}$$

In principle the right hand side of equation (65) is determined, but it is typical to encounter singularities in the derivative $\dot{J}_E$. DSSP50 avoids numerical difficulties by approximating the derivative by that of a lightly damped error signal J'_E:

$$k_1\, \dot{J}'_E + k_2\, J'_E = J_E \tag{66}$$

so that

$$J_C = \left(K_P + \frac{K_D}{k_1}\right) J_E + K_I \int J_E\, dt - K_D \left(\frac{k_2}{k_1}\right) J'_E \tag{67}$$

The integral term in equation (67) and the damped error signal J'_E are obtained by integrating the first order equations:

$$\begin{aligned} \frac{d}{dt}\int J_E\, dt &= J_E \\ \frac{d}{dt} J'_E &= \frac{1}{k_1} J_E - \frac{k_2}{k_1} J'_E \end{aligned} \tag{68}$$

Control signals are clipped at ± 1 and multiplied by a control gain C_C in appropriate units. An example of autopilot responses to two idealized error signals is shown in figure 12.

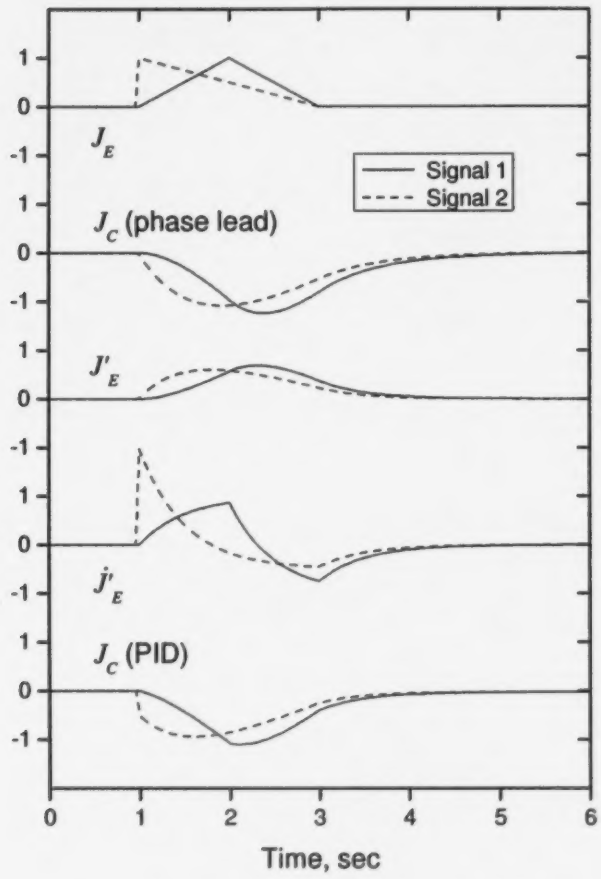

Figure 12. Autopilot response to two short error signals: (1) a ramp-up/ramp-down and (2) a step-up/ramp-down. Phase lead parameters are $\alpha = 3$ and $\tau = 2$. PID parameters are $k_1 = 0.5$, $k_2 = 1$, $K_P = -1.5$, $K_I = -0.02$, and $K_D = 0.5$.

The program provides default values for phase lead parameters α and τ, and for PID coefficients k_1, k_2, K_P, K_I, and K_D, but to optimize these quantities requires some trial-and-error. Error and control signal time histories are listed on the auxiliary output file for a free manoeuver to aid the process. Error and control gains, C_E and C_C, should be similarly optimized.

In evaluating controllability note that in some cases the control mechanism may not have sufficient authority to meet the desired criterion even if the autopilot has been optimized. For instance, differentially deflected tailplanes are typically not sufficient to achieve effective roll control.

11 Plane Reversal

The derivation of plane reversal speed is outlined in reference [32]. It applies to planes for pitch and heave control that are located aft of the heave neutral point; that is, for sternplanes and generally for sailplanes, but generally not for bowplanes. For example, suppose a downward force is applied to the sternplanes. Above plane reversal speed $U_{c\delta}$ the submarine pitches up and rises; this is the normal speed regime. Below $U_{c\delta}$ it still pitches up but descends, and exactly at $U_{c\delta}$ it pitches up but depth remains constant.

$U_{c\delta}$ is typically a few knots. From small perturbation analysis it is given by:

$$U_{c\delta} = \sqrt{g\overline{BG}\,\frac{m'}{Z'_w x'_\delta + M'_w}} \tag{69}$$

where m' is nondimensional mass, x'_δ is the nondimensional longitudinal location of the control plane, and Z'_w and M'_w are hydrodynamic coefficients. The `PReverse` option in a `DSSP50 Coef` simulation generates an estimate of $U_{c\delta}$.

Clearly, plane reversal will compromise controllability if it is not accounted for. A simple technique, used in `DSSP50` for both appendages and lumps, is to introduce an additional control gain that changes sign, and magnitude if required, according to whether vehicle speed is above or below plane reversal speed. A typical gain profile to achieve this is illustrated in figure 13.

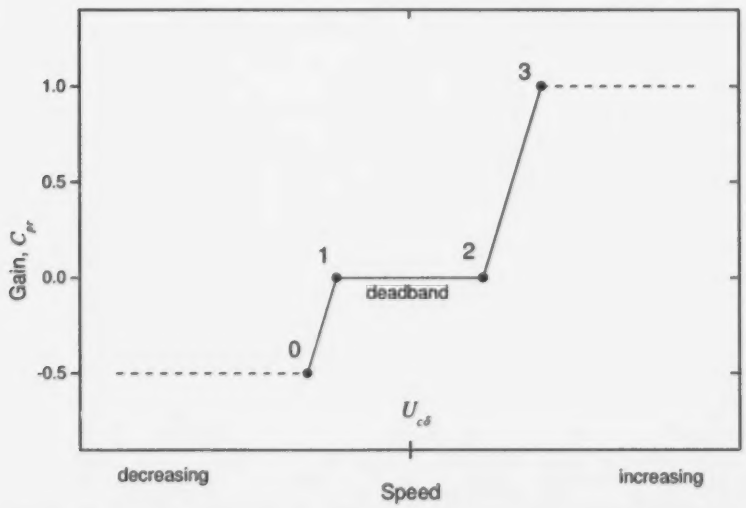

Figure 13. Plane reversal compensation: a typical four-point gain profile for aft control planes. Gains for forward planes are descending.

12 Compression

In free simulations and MLD calculations, loss of buoyancy due to compression of the pressure hull and resilient tiles or cladding on the vessel is calculated, with a few modifications, by the method used in DSSP40. The user provides a table of loss of buoyant mass (positive) and effective location versus depth for the hull, and another for the tiles. The tiles are assumed to compress no further past the last depth given, but the hull is assumed to compress indefinitely. The compression parameters are illustrated in figure 14. Values for zero depth are inferred as shown.

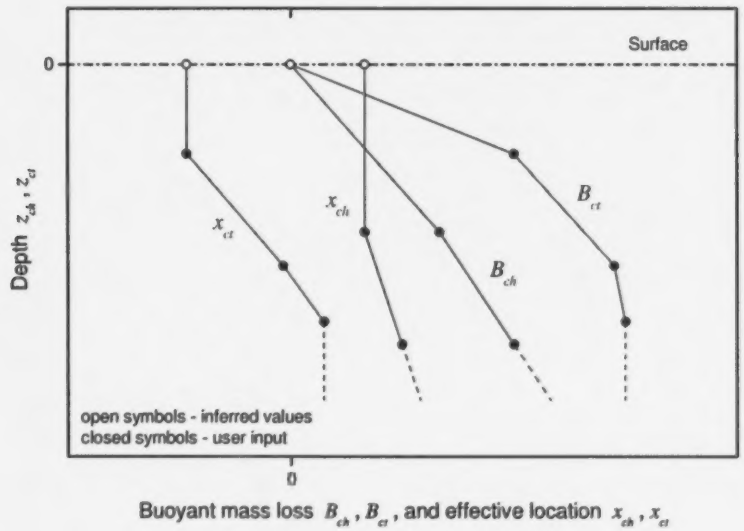

Figure 14. Compression parameters. Discrete values of hull buoyant mass loss $B_{ch}(z_{ch})$ and location $x_{ch}(z_{ch})$, and corresponding quantities for resilient tiles, $B_{ct}(z_{ct})$ and $x_{ct}(z_{ct})$, are user-supplied.

Compression is accounted for in initializing the simulations, so that the vessel is truly neutrally buoyant at the initial depth.

13 Blowing Main Ballast

The algorithms for blowing main ballast tanks are modifications of the model used in DSSP02 [31]. The tanks are assumed to be initially completely flooded and ballast is blown out by high pressure air from an associated bottle group [2].

The classical analysis of ideal gas flow through a choked isentropic nozzle leads to the approximation that the mass flow rate from the HP air system, $\dot{m}_{HP}$, is proportional to the mass of air remaining in the bottle group [33]. The mass flow rate is:

$$\frac{d}{dt} m_{HP} = \dot{m}_{HP\bullet} \left[1 - \frac{m_{HP}}{m_{HP\bullet}} \right] \tag{70}$$

where the subscript $\bullet$ indicates, as elsewhere in this report, initial conditions, and the mass of air released from the HP air system is:

$$m_{HP}(t) = m_{HP\bullet} \left[1 - \exp\left(- \frac{\dot{m}_{HP\bullet}}{m_{HP\bullet}} t \right) \right] \tag{71}$$

Itard cites [34] an alternative expression for one-dimensional choked flow in which the decay term depends on γ, the ratio of specific heats at constant pressure and volume:

$$m_{HP}(t) = m_{HP\bullet} \left[1 - \left(1 + \frac{\gamma - 1}{2} \frac{\dot{m}_{HP\bullet}}{m_{HP\bullet}} t \right)^{\frac{-2}{\gamma - 1}} \right] \tag{72}$$

For typical initial conditions $\dot{m}_{HP\bullet}$ and $m_{HP\bullet}$, and assuming that γ is a constant equal to 1.4 for air, equations (71) and (72) give very similar results. The algorithm implemented in DSSP50 is the exponential form.

The isentropic flow relationship between pressure $P(t)$ and specific volume $\mathcal{V}(t)$, $P\mathcal{V}^{\gamma} = \text{constant}$, leads to the following expression for pressure in the bottle group:

$$P_{HP}(t) = P_{HP\bullet} \left[1 - \frac{m_{HP}(t)}{m_{HP\bullet}} \right]^{\gamma} \tag{73}$$

Initial conditions given for ballast tank blowing are pressure in the bottle group, $P_{HP\bullet}$, and blowing rate, $\dot{m}_{HP\bullet}$, which is determined by the nozzle. The initial mass of air in the bottle group can be estimated from its volume V_{HP} using the ideal gas equation:

$$m_{HP\bullet} = \frac{P_{HP\bullet} V_{HP}}{R T_{HP\bullet}} \tag{74}$$

R is the gas constant for air and $T_{HP\bullet}$ is the initial temperature of the bottle group, in general equal to seawater ambient temperature.

Air pressure downstream of the nozzle, in the ballast tank being blown, is determined by depth, z_{0BT}:

$$P_{BT}(z_{0BT}) = P_{atm} + \rho g z_{0BT} \tag{75}$$

where P_{atm} is atmospheric pressure, ρ is water density, and z_{0BT} is depth to the water surface in the tank (simplified by using the centroid of the fully-blown tank).

The assumption of choked flow through the nozzle is valid so long as the ratio of pressures on each side of the nozzle, P_{HP}/P_{BT}, is greater than the critical pressure ratio r'_P [35]:

$$r'_P = \left(\frac{2}{1 + \gamma} \right)^{\frac{\gamma}{1 - \gamma}} \tag{76}$$

which is 1.8929 for $\gamma = 1.4$. When P_{HP} has dropped sufficiently for r'_P to be reached, the amount of air remaining in the bottle groups is for practical purposes negligible, and discrepancies that arise if the blow is not stopped can be ignored.

It remains to calculate the volume of air in the ballast tank as a function of time. The simplest, and most common, assumption is that the air blown into the tank instantly expands at ambient pressure P_{BT} and temperature $T_{BT\bullet}$, as in references [31,33]. This model can be characterized as isothermal. The density of air under these conditions is:

$$\rho_{air}(z_{0BT}) = \frac{P_{BT}(z_{0BT})}{R T_{BT\bullet}} \tag{77}$$

and the volume of released air, V_{BT} is:

$$V_{BT}(z_{0BT}, t) = \frac{m_{HP}(t)}{\rho_{air}(z_{0BT})} \tag{78}$$

V_{BT} is limited by the maximum available volume, which is a function of pitch and the geometry of the flooding holes in the bottom of the tank. In DSSP50, tanks are assumed to be spherical with a single opening in the bottom for the purpose of estimating this correction. After the correction to V_{BT}, the resulting buoyancy force is:

$$B(z_{0BT}, t) = [\rho - \rho_{air}(z_{0BT})]\, g\, V_{BT}(z_{0BT}, t) \tag{79}$$

For the high bottle group pressures used in submarine ballast blowing systems, air is released into the tank at temperatures considerably less than the ambient temperature, and the isothermal model will overpredict its volume. A better approximation may be that the process is adiabatic, i.e., temperature of the released air is taken account of, but heat transfer between the bottle group, the ballast tank, and their respective surroundings is not, so the air remains cold for the duration of the blow and thereafter. (This is equivalent to the assumption that the time scale for heat transfer between the system and its surroundings is significantly longer than the duration of the blow and the additional time until the simulation is stopped.) With this approximation the volume of air in the ballast tank is likely to be underpredicted. Nevertheless, for a typical simulation the adiabatic model may be closer to reality than the isothermal one.

As the adiabatic blow proceeds, air temperature in the bottle group, and hence that of the air entering the nozzle, drops according to:

$$T_{HP}(t) = \frac{P_{HP}(t)\, V_{HP}}{(m_{HP\bullet} - m_{HP}(t))\, R} \tag{80}$$

The temperature drops further in the throat of the nozzle. Air entering the tank is assumed to be at this lower temperature, which for choked flow [35] is:

$$T_{BT}(t) = \frac{2}{1+\gamma} T_{HP}(t) \tag{81}$$

The corresponding density of air entering the tank is:

$$\rho_{air}(z_{0BT}, t) = \frac{P_{BT}(z_{0BT})}{R T_{BT}(t)} \tag{82}$$

and we can approximate V_{BT} by:

$$V_{BT}(z_{0BT}, t) = \int_0^t \frac{\dot{m}_{HP}(t)}{\rho_{air}(z_{0BT}, t)}\, dt \tag{83}$$

subject to the maximum available volume noted above. To obtain the resulting buoyancy force we define the net density of air contained in the ballast tank, $\overline{\rho}_{air}$, as:

$$\overline{\rho}_{air}(z_{0BT}, t) = \frac{m_{BT}(t)}{V_{BT}(z_{0BT}, t)} \tag{84}$$

where $m_{BT}(t)$ is $m_{HP}(t)$ adjusted to correspond to V_{BT} if the latter is limited. Then

$$B(z_{0BT}, t) = [\rho - \overline{\rho}_{air}(z_{0BT}, t)]\, g\, V_{BT}(z_{0BT}, t) \tag{85}$$

In addition to the assumption of no heat transfer between the bottle group, the ballast tank, and their respective surroundings, there are a number of other approximations worth noting. In reality, the specific heat ratio γ is not constant over the ranges of pressure and temperature encountered in blowing ballast at great depth and could be replaced by $\gamma(P,T)$, albeit with some increase in computational complexity since some of the relations in the equations above then become recursive. The limiting effect, if any, of a pressure gradient across the ballast tank flooding holes is ignored: ballast expulsion from the tank is assumed to be instantly equal to V_{BT} and there is therefore no calculation of overpressure in the tank. Practical considerations such as pipe losses can be neglected as long as there is choked flow at the nozzle.

Although most of these additional aspects of the problem can be modeled in some fashion, at present there is a disincentive to further elaborating the calculation in DSSP50 in that there are, to the author's knowledge, no suitable data for validation.

Blowing is integrated in time using first order equation (70) for each HP air bottle group, and by:

$$\frac{d}{dt} V_{BT} = \frac{\dot{m}_{BT} - \dot{m}_{BV}}{\overline{\rho}_{air}} \tag{86}$$

for each main ballast tank. For venting, the constant venting rate $\dot{m}_{BV}$ is incorporated as shown.

Estimated time histories of bottle group pressure and temperature, and of ballast tank buoyancy force, are listed on the auxiliary output file for a free vehicle simulation.

The comparison between blowing models in figure 15 demonstrates that the difference between them can be significant, although it is somewhat exaggerated in this example by artificially canceling the effect of the additional buoyancy on depth.

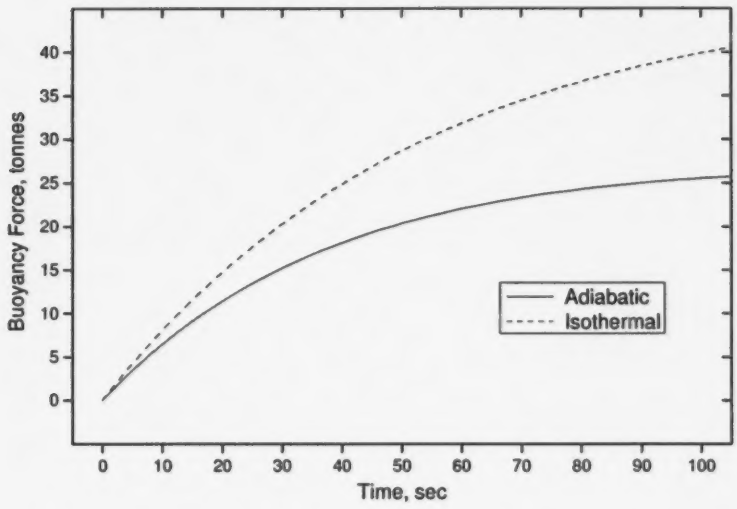

Figure 15. A comparison between blowing models. The MBT was blown while holding depth constant and the pitch at zero.

14 Compartment Flooding

The standard equation for mass flow through a flood hole [31] is integrated directly in time:

$$\frac{d}{dt} m_F = \frac{\pi D_F^2}{4} \rho \sqrt{2 g z_{0F}}\, C_F \tag{87}$$

where D_F is the diameter of the breach (assumed circular) causing the flood, z_{0F} is the depth of the breach approximated by that of the centroid of the watertight compartment involved, and C_F is the coefficient of discharge.

The centroid of the flood water is calculated, rather than simply using the centroid of the compartment for example, because it varies significantly with the amount on board and with the angle of pitch, figure 16. In DSSP50, a watertight compartment is modeled as a circular cylinder characterized by occupancy, O_C, which is the fraction of its volume not available for flooding. The maximum amount of floodwater that can enter is $(1 - O_C)$ times the empty volume of the cylinder.

Modeling flood water this way allows an approximate representation of how its mass moves: from forward to aft as pitch changes from negative to positive, for example.

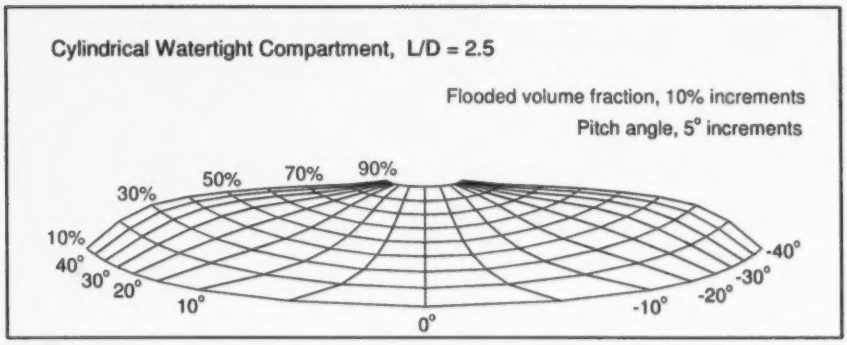

Figure 16. The centroid of floodwater in a watertight compartment; the boundary indicates the centerline profile of the compartment. Flooded volume fraction is the fraction of the available volume. Forward is to the right.

This level of detail is likely significant for vehicle dynamics especially if the flooded compartment is situated about midships, but was not considered to be necessary in modeling ballast tanks during a blow.

Estimated time histories of floodwater in each compartment are listed on the auxiliary output file for a free vehicle simulation.

15 Trim and Compensation

Trimming is the action of transferring water between tanks in order to achieve zero pitch and roll on the submarine under static conditions. Compensating is transferring water between tanks and the sea in order to achieve neutral buoyancy. In DSSP50, both are done at a constant rate assumed to be determined by pump capacity, so additional differential equations are not required.

16 Variable Mass

A number of operations, including ballast blowing and compartment flooding, result in changes in weight and CG in the equations of motion. (In some formulations, blowing is equated with a change in buoyancy, but that is equivalent so long as the accounting is done correctly in each case.) In addition, attendant changes in net mass and mass distribution make the inertial properties $(m, I_x, \ldots)$ in the equations functions of time, and also result in terms in $\dot{m}$, etc., in equations (2), (3), and following. In practice the

latter can generally be ignored, since even if all the ballast is blown simultaneously the contribution of these terms to the dynamics of a submarine is likely to be negligible. Variation of the inertial properties is often also ignored. The change in net mass for a full ballast blow, proportional to the reserve of buoyancy, is typically 10–15 percent of the total for a modern submarine. A full blow is required in either the last stages of a normal surfacing evolution or, from depth, for the purpose of emergency recovery. In the first case accelerations are small, and in the second the submarine is typically in a more-or-less steady rise, and accelerations have dropped, by the time the change in inertial properties is more than a few percent. For marginal recoveries, however, correctly modeling inertia for acceleration terms in the equations of motion may be important.

As discussed in the user guide and below, variation of the inertial properties requires recalculation and inversion of the inertial plus added mass matrix, $(\mathbf{I}+\mathbf{A})$, at each time step. Full accounting for inertial changes is the default in `DSSP50`, but to avoid any additional computational overhead the user can include a `NoMass` input record, which suppresses all calculations other than the basic changes in weight and CG. It is easy to establish the effect of this simplification with a few trial simulations.

For a detailed discussion of how the equations of motion are modified by accounting for variation in mass and moments of inertia, see Strumpf [36]. Note the convention in Strumpf that cross products of inertia are unsigned, unlike the more standard usage of Abkowitz [3] and others. Additional terms for changing inertial properties are included in the state variable equations discussed in section 17.1.

17 Integrating the Equations of Motion

This section applies to simulating free manoeuvers and to MLD calculation, which consists of a series of free runs. Some issues particular to MLDs are discussed in the next section.

17.1 The State Variable Equations

The left hand sides of the state variable equations in `DSSP50` have the standard form [3,7] with the addition of inertial rate-of-change terms $\dot{m}(\ldots)$, $\dot{I}_x(\ldots)$, etc.

Surge equation:

$$\begin{aligned} & m\left[\dot{u}-vr+wq-y_G\left(\dot{r}-pq\right)+z_G\left(\dot{q}+rp\right)-x_G\left(q^2+r^2\right)\right]- \\ & \tfrac{1}{2}\rho\ell^3\left[X'_{\dot{u}}\dot{u}+X'_{\dot{v}}\dot{v}+X'_{\dot{w}}\dot{w}\right]-\tfrac{1}{2}\rho\ell^4\left[X'_{\dot{p}}\dot{p}+X'_{\dot{q}}\dot{q}+X'_{\dot{r}}\dot{r}\right]+ \\ & \dot{m}\left(u-y_G r+z_G q\right) \\ & \qquad\qquad = \; X(\mathbf{u})+P_X(\mathbf{u})-(W-B)\sin\theta+X_\bullet \end{aligned} \tag{88}$$

Sway equation:

$$
\begin{aligned}
& m\left[\dot{v}-wp+ur-z_G\left(\dot{p}-qr\right)+x_G\left(\dot{r}+pq\right)-y_G\left(r^2+p^2\right)\right]- \\
& \tfrac{1}{2}\rho\ell^3\left[X'_{\dot{v}}\dot{u}+Y'_{\dot{v}}\dot{v}+Y'_{\dot{w}}\dot{w}\right]-\tfrac{1}{2}\rho\ell^4\left[Y'_{\dot{p}}\dot{p}+Y'_{\dot{q}}\dot{q}+Y'_{\dot{r}}\dot{r}\right]+ \\
& \dot{m}\left(v-z_Gp+x_Gr\right) \\
& \qquad = Y(\mathbf{u})+P_Y(\mathbf{u})+(W-B)\sin\phi\cos\theta+Y_{\bullet}
\end{aligned}
\tag{89}
$$

Heave equation:

$$
\begin{aligned}
& m\left[\dot{w}-uq+vp-x_G\left(\dot{q}-rp\right)+y_G\left(\dot{p}+qr\right)-z_G\left(p^2+q^2\right)\right]- \\
& \tfrac{1}{2}\rho\ell^3\left[X'_{\dot{w}}\dot{u}+Y'_{\dot{w}}\dot{v}+Z'_{\dot{w}}\dot{w}\right]-\tfrac{1}{2}\rho\ell^4\left[Z'_{\dot{p}}\dot{p}+Z'_{\dot{q}}\dot{q}+Z'_{\dot{r}}\dot{r}\right]+ \\
& \dot{m}\left(w-x_Gq+y_Gp\right) \\
& \qquad = Z(\mathbf{u})+P_Z(\mathbf{u})+(W-B)\cos\phi\cos\theta+Z_{\bullet}
\end{aligned}
\tag{90}
$$

Roll equation:

$$
\begin{aligned}
& I_x\dot{p}-\left(I_y-I_z\right)qr-I_{xy}\left(\dot{q}-rp\right)-I_{xz}\left(\dot{r}+pq\right)-I_{yz}\left(q^2-r^2\right)+ \\
& m\left[y_G\left(\dot{w}-uq+vp\right)-z_G\left(\dot{v}-wp+ur\right)\right]- \\
& \tfrac{1}{2}\rho\ell^4\left[X'_{\dot{p}}\dot{u}+Y'_{\dot{p}}\dot{v}+Z'_{\dot{p}}\dot{w}\right]-\tfrac{1}{2}\rho\ell^5\left[K'_{\dot{p}}\dot{p}+K'_{\dot{q}}\dot{q}+K'_{\dot{r}}\dot{r}\right]+ \\
& \dot{I}_xp-\dot{I}_{xy}q-\dot{I}_{xz}r+\dot{m}\left(y_Gw-z_Gv\right) \\
& \qquad = K(\mathbf{u})+P_K(\mathbf{u})+ \\
& \qquad\quad \left(y_GW-y_BB\right)\cos\phi\cos\theta-\left(z_GW-z_BB\right)\sin\phi\cos\theta+K_{\bullet}
\end{aligned}
\tag{91}
$$

Pitch equation:

$$
\begin{aligned}
& I_y\dot{q}-\left(I_z-I_x\right)rp-I_{yz}\left(\dot{r}-pq\right)-I_{xy}\left(\dot{p}+qr\right)-I_{xz}\left(r^2-p^2\right)+ \\
& m\left[z_G\left(\dot{u}-vr+wq\right)-x_G\left(\dot{w}-uq+vp\right)\right]- \\
& \tfrac{1}{2}\rho\ell^4\left[X'_{\dot{q}}\dot{u}+Y'_{\dot{q}}\dot{v}+Z'_{\dot{q}}\dot{w}\right]-\tfrac{1}{2}\rho\ell^5\left[K'_{\dot{q}}\dot{p}+M'_{\dot{q}}\dot{q}+M'_{\dot{r}}\dot{r}\right]+ \\
& \dot{I}_yq-\dot{I}_{yz}r-\dot{I}_{xy}p+\dot{m}\left(z_Gu-x_Gw\right) \\
& \qquad = M(\mathbf{u})+P_M(\mathbf{u})- \\
& \qquad\quad \left(z_GW-z_BB\right)\sin\theta-\left(x_GW-x_BB\right)\cos\phi\cos\theta+M_{\bullet}
\end{aligned}
\tag{92}
$$

Yaw equation:

$$
\begin{aligned}
& I_z\dot{r}-\left(I_x-I_y\right)pq-I_{xz}\left(\dot{p}-qr\right)-I_{yz}\left(\dot{q}+rp\right)-I_{xy}\left(p^2-q^2\right)+ \\
& m\left[x_G\left(\dot{v}-wp+ur\right)-y_G\left(\dot{u}-vr+wq\right)\right]- \\
& \tfrac{1}{2}\rho\ell^4\left[X'_{\dot{r}}\dot{u}+Y'_{\dot{r}}\dot{v}+Z'_{\dot{r}}\dot{w}\right]-\tfrac{1}{2}\rho\ell^5\left[K'_{\dot{r}}\dot{p}+M'_{\dot{r}}\dot{q}+N'_{\dot{r}}\dot{r}\right]+ \\
& \dot{I}_zr-\dot{I}_{xz}p-\dot{I}_{yz}q+\dot{m}\left(x_Gv-y_Gu\right) \\
& \qquad = N(\mathbf{u})+P_N(\mathbf{u})+ \\
& \qquad\quad \left(x_GW-x_BB\right)\sin\phi\cos\theta+\left(y_GW-y_BB\right)\sin\theta+N_{\bullet}
\end{aligned}
\tag{93}
$$

Other terms related to mass change, e.g., in $\dot{x}_G$, etc. [36], have been neglected. We have used the added mass identities for ideal potential flow [37]: $Y'_{\dot{u}} = X'_{\dot{v}}, \ldots, N'_{\dot{q}} = M'_{\dot{r}}$. Hydrodynamic load vector $\mathbf{F}(\mathbf{u})$ has been separated into components $X(\mathbf{u}), \ldots, N(\mathbf{u})$, and propulsion vector $\mathbf{P}(\mathbf{u})$ into components $P_X(\mathbf{u}), \ldots, P_N(\mathbf{u})$.

Constant loads $X_\bullet, \ldots, N_\bullet$ establish initial neutral buoyancy and zero trim:

$$\begin{aligned} X_\bullet &= -(P_X + X_*)_\bullet \\ &\vdots \\ N_\bullet &= -(P_N + N_*)_\bullet \end{aligned} \tag{94}$$

where $X_*, \ldots, N_*$ comprise the static hydrodynamic loads for straight-ahead level flight and any externally imposed loads. The subscript $\bullet$ denotes initial conditions. $X_\bullet, \ldots, N_\bullet$ are calculated during initialization of the propulsors.

Equations (88) to (93) are coupled in the derivatives of the state variables. Rearranging terms, they can be written as:

$$\frac{d}{dt}\mathbf{u} = \mathbf{M}^{-1}\,\mathbf{Q}\,(\mathbf{u}, t) \tag{95}$$

where all the non-acceleration terms are collected in the generic load vector $\mathbf{Q}$ and $\mathbf{M}$ is what we have called the inertial plus added mass matrix:

$$\mathbf{M} = \mathbf{I} + \mathbf{A} \tag{96}$$

$\mathbf{I}$ is the inertial matrix:

$$\mathbf{I} = \begin{bmatrix} m & 0 & 0 & 0 & mz_G & -my_G \\ 0 & m & 0 & -mz_G & 0 & mx_G \\ 0 & 0 & m & my_G & -mx_G & 0 \\ 0 & -mz_G & my_G & I_x & -I_{xy} & -I_{xz} \\ mz_G & 0 & -mx_G & -I_{xy} & I_y & -I_{yz} \\ -my_G & mx_G & 0 & -I_{xz} & -I_{yz} & I_z \end{bmatrix} \tag{97}$$

and $\mathbf{A}$ is the added mass and moment matrix:

$$\mathbf{A} = -\begin{bmatrix} X_{\dot{u}} & X_{\dot{v}} & X_{\dot{w}} & X_{\dot{p}} & X_{\dot{q}} & X_{\dot{r}} \\ X_{\dot{v}} & Y_{\dot{v}} & Y_{\dot{w}} & Y_{\dot{p}} & Y_{\dot{q}} & Y_{\dot{r}} \\ X_{\dot{w}} & Y_{\dot{w}} & Z_{\dot{w}} & Z_{\dot{p}} & Z_{\dot{q}} & Z_{\dot{r}} \\ X_{\dot{p}} & Y_{\dot{p}} & Z_{\dot{p}} & K_{\dot{p}} & K_{\dot{q}} & K_{\dot{r}} \\ X_{\dot{q}} & Y_{\dot{q}} & Z_{\dot{q}} & K_{\dot{q}} & M_{\dot{q}} & M_{\dot{r}} \\ X_{\dot{r}} & Y_{\dot{r}} & Z_{\dot{r}} & K_{\dot{r}} & M_{\dot{r}} & N_{\dot{r}} \end{bmatrix} \tag{98}$$

The elements of $\mathbf{A}$ are dimensioned: $X_{\dot{u}} = \frac{1}{2}\rho\ell^3 X'_{\dot{u}}$ and so on. We may be able to further simplify matrix $\mathbf{A}$ since many of the off-diagonal elements become zero if the vehicle has port-starboard symmetry and if the hydrodynamic reference (about which

moments are taken and rotation evaluated) is on the symmetry plane [37]. However, DSSP50 does not impose symmetry and allows an arbitrary location to be the reference, so the full form of **A** is retained. Identities in ideal potential flow relating the added masses to other manoeuvering coefficients, such as $X'_{wq} = Z'_{\dot{w}}$ [37], can be used for terms in **Q** in a coefficient model.

17.2 Inverting the I+A Matrix

Since **A** is effectively constant for submerged vehicles, so is **M** when the inertial properties are constant, and **M** has only to be inverted once, initially, to evaluate equation (95) for the rest of the time simulation. But unless we adopt the approximation that only weight, W, changes during ballast blowing and flooding, these actions result in variation of the inertial properties, and **M** must be inverted at each timestep. This does not appear to be a problem as computational overhead for the inversion is small.

In DSSP50 build 090910 the elements of **M** are dimensioned, which has the potential for making the matrix ill-conditioned for inversion, but so long as the hydrodynamic reference is in the vicinity of CB and CG this is unlikely to be a problem since the off-diagonal elements are thereby close to zero. If regular inversion fails because of ill-conditioning, whether due to shifting the reference or to a peculiarity of vehicle geometry, the user can invoke the Singular Value Decomposition [38] option with a `SVDecomp` record. Unfortunately this solution is limited in its effectiveness, and has the caveat that some accuracy is lost. Reference [1] discusses the better solution of replacing a shifted reference, if that is the cause, by assigning a target point.

17.3 Trajectory and Attitude

Free and MLD simulations track the trajectory and attitude of the submarine. This requires transformations between the earth-fixed axis and body-fixed reference axis, figure 1. To obtain the trajectory, (x_0, y_0, z_0), we integrate

$$\frac{d}{dt}\begin{bmatrix} x_0 \\ y_0 \\ z_0 \end{bmatrix} = \mathbf{L}^{-1}\begin{bmatrix} u \\ v \\ w \end{bmatrix} \tag{99}$$

where

$$\mathbf{L} = \begin{bmatrix} l_1 & l_2 & l_3 \\ m_1 & m_2 & m_3 \\ n_1 & n_2 & n_3 \end{bmatrix} \tag{100}$$

is the transformation matrix to rotate the earth axis into the body axis.

Orientation of the body axis with respect to the earth axis is generally expressed in terms of the three Euler angles (ϕ, θ, ψ). To this point we have used these angles in the extended state vector, and in equations (88) to (93) to represent orientation of

the weight and buoyancy forces. Euler angles are conventionally defined by doing the individual rotations in reverse order: yaw ψ, pitch θ, and finally roll ϕ.

In terms of Euler angles the elements of $\mathbf{L}$ are [3]:

$$\begin{aligned} l_1 &= \cos\theta\cos\psi \\ l_2 &= \cos\theta\sin\psi \\ l_3 &= -\sin\theta \\ m_1 &= -\cos\phi\sin\psi + \sin\phi\sin\theta\cos\psi \\ m_2 &= \cos\phi\cos\psi + \sin\phi\sin\theta\sin\psi \\ m_3 &= \sin\phi\cos\theta \\ n_1 &= \sin\phi\sin\psi + \cos\phi\sin\theta\cos\psi \\ n_2 &= -\sin\phi\cos\psi + \cos\phi\sin\theta\sin\psi \\ n_3 &= \cos\phi\cos\theta \end{aligned} \tag{101}$$

And to obtain Euler angle time histories we integrate the rotational rates:

$$\frac{d}{dt}\begin{bmatrix} \phi \\ \theta \\ \psi \end{bmatrix} = \begin{bmatrix} p + \dot{\psi}\sin\theta \\ q\cos\phi - r\sin\phi \\ \dfrac{r\cos\phi + q\sin\phi}{\cos\theta} \end{bmatrix} \tag{102}$$

with initial rates and angles input by the user.

The difficulty with the Euler angle formulation is that $\dot{\phi}$ and $\dot{\psi}$ are singular when $\theta = \pm\pi/2$, so roll and yaw are indeterminate when the submarine is pitched vertically up or down. This condition is known as gimbal lock. While vertical pitch is unlikely to be (and hopefully, never) reached with a submarine, it may well occur with small UUVs. For any underwater vehicle, it is desirable to avoid the possibility of gimbal lock in a simulation that is used to evaluate extreme manoeuvers.

DSSP50 uses a quaternion model of the rotational transformation [39] to avoid the problem. Before discussing it we will generalize the transformation of the gravity vector into body axes that has resulted in the appearance of the Euler angles in the weight and buoyancy terms of equations (88) to (93). The general form of these terms, to which any model of the transformation matrix $\mathbf{L}$ is applicable, is:

$$\begin{aligned} &\text{Surge equation:} && \ldots + (W-B)l_3 + \ldots \\ &\text{Sway equation:} && \ldots + (W-B)m_3 + \ldots \\ &\text{Heave equation:} && \ldots + (W-B)n_3 + \ldots \\ &\text{Roll equation:} && \ldots + (y_G W - y_B B)n_3 - (z_G W - z_B B)m_3 + \ldots \\ &\text{Pitch equation:} && \ldots + (z_G W - z_B B)l_3 - (x_G W - x_B B)n_3 + \ldots \\ &\text{Yaw equation:} && \ldots + (x_G W - x_B B)m_3 - (y_G W - y_B B)l_3 + \ldots \end{aligned} \tag{103}$$

In the quaternion model, the three Euler angles are replaced by four parameters (e_0, e_1, e_2, e_3) with the constraint:

$$e_0^2 + e_1^2 + e_2^2 + e_3^2 = 1 \tag{104}$$

These are called the Euler-Rodrigues symmetric parameters in reference [39]. The elements of transformation matrix **L**, expressed in quaternion parameters, are:

$$\begin{aligned} l_1 &= e_0^2 + e_1^2 - e_2^2 - e_3^2 \\ l_2 &= 2(e_1 e_2 + e_0 e_3) \\ l_3 &= 2(e_1 e_3 - e_0 e_2) \\ m_1 &= 2(e_1 e_2 - e_0 e_3) \\ m_2 &= e_0^2 - e_1^2 + e_2^2 - e_3^2 \\ m_3 &= 2(e_2 e_3 + e_0 e_1) \\ n_1 &= 2(e_1 e_3 + e_0 e_2) \\ n_2 &= 2(e_2 e_3 - e_0 e_1) \\ n_3 &= e_0^2 - e_1^2 - e_2^2 + e_3^2 \end{aligned} \tag{105}$$

And the quaternion time history is obtained by integrating:

$$\frac{d}{dt}\begin{bmatrix} e_0 \\ e_1 \\ e_2 \\ e_3 \end{bmatrix} = \frac{1}{2}\begin{bmatrix} -e_1 p - e_2 q - e_3 r \\ e_0 p - e_3 q + e_2 r \\ e_3 p + e_0 q - e_1 r \\ -e_2 p + e_1 q + e_0 r \end{bmatrix} \tag{106}$$

Renormalization of the parameters at each time step to enforce equation (104) avoids orthogonality errors in the integration. The quaternions corresponding to initial Euler angles (ϕ, θ, ψ) are [38]:

$$\begin{aligned} e_0 &= \cos\frac{\phi}{2}\cos\frac{\theta}{2}\cos\frac{\psi}{2} + \sin\frac{\phi}{2}\sin\frac{\theta}{2}\sin\frac{\psi}{2} \\ e_1 &= \sin\frac{\phi}{2}\cos\frac{\theta}{2}\cos\frac{\psi}{2} - \cos\frac{\phi}{2}\sin\frac{\theta}{2}\sin\frac{\psi}{2} \\ e_2 &= \cos\frac{\phi}{2}\sin\frac{\theta}{2}\cos\frac{\psi}{2} + \sin\frac{\phi}{2}\cos\frac{\theta}{2}\sin\frac{\psi}{2} \\ e_3 &= \cos\frac{\phi}{2}\cos\frac{\theta}{2}\sin\frac{\psi}{2} - \sin\frac{\phi}{2}\sin\frac{\theta}{2}\cos\frac{\psi}{2} \end{aligned} \tag{107}$$

The quaternion model clearly has no singularities, and gimbal lock does not occur. For output from the program it is desirable to reconstruct the Euler angles even though they no longer take part in the calculations. They are derived from equations (101). Pitch is returned in the range $-\pi/2 \leq \theta \leq \pi/2$. The angles ϕ and ψ are set to zero where they are indeterminate:

$$\begin{aligned} \phi &= \tan^{-1}\left(\frac{m_3}{n_3}\right) && \text{if } n_3 \neq 0 \\ &= 0 && \text{otherwise} \end{aligned} \tag{108}$$

$$\theta = \sin^{-1}(-l_3) \tag{109}$$

$$\begin{aligned} \psi &= \tan^{-1}\left(\frac{l_2}{l_1}\right) && \text{if } l_1 \neq 0 \\ &= 0 && \text{otherwise} \end{aligned} \tag{110}$$

Another advantage claimed for the quaternion model is efficiency [39]. `DSSP50` currently allows the user to select Euler angles over the default quaternion model by using a `GimbaLock Euler` record [2]. Comparison between the two models generally shows little difference in efficiency between them for simulations up to several hundred seconds, likely because other calculations in the time integral dominate the computational effort. A modest advantage for the quaternion model has been observed in some cases where integration tolerance and timestep limits have been fine-tuned. The optional Euler angle model will likely be dropped from a future build of the code.

17.4 Integration Methods

There are two methods for integrating the equations of motion and various auxiliary differential equations over time. The first is Nørsett's order (3,4) Runge-Kutta algorithm with adaptive timestep for local error control [40,41]. Output can be interpolated to regular timesteps, but calculations always use the irregular adaptive steps. The user may specify a minimum timestep, maximum timestep, and error tolerance for the integration.

The second integration method is to use a first-order Adams-Bashforth predictor (i.e., the first stage of the Adams-Moulton Predictor-Corrector Method [42]). This was the method used in `DSSP40`. Local errors are not controlled, which means that the fixed timestep should be kept small, and will likely be unnecessarily small for simple tactical manoeuvers. However, with the program defaults, Adams-Bashforth may give comparable accuracy while being somewhat faster than Nørsett for manoeuvers in which mass is changing or the autopilots are heavily used.

The preceding sections have presented each member of the system of equations to be integrated so that the system as a whole is in canonical form: $\dot{\mathbf{Y}} = \mathbf{K}(\dot{\mathbf{Y}}, \mathbf{Y}, t)$, in which matrix $\mathbf{K}$ describes the dynamics of the total system $\mathbf{Y}$ such that the individual equations are uncoupled on the left hand side. In `DSSP50` build 090910 there are 103 equations in the system. Up to 100 of them will be active depending on the configuration of the vehicle and options selected by the user; the others are zeroed on the right hand side. The system is summarized in table 2 in order of index i in the vector $\mathbf{Y} = (Y_1, \ldots, Y_i, \ldots)^T$.

The vector of system and motion derivatives, $\dot{\mathbf{Y}}$, is updated in subroutine `DYDT` and in the subroutines it calls, `AUTODOIT`, `BLOWVENT`, and `FLOOD`. In Nørsett's method this occurs four times every attempted timestep.

Table 2. System of equations integrated in a free manoeuver or MLD simulation. Indices depend on component limits in the program, and may change in future builds. Either the Euler angle or quaternion equations will be active, but not both.

Index in $\mathbf{Y}$ i	What	Equation(s)
1,2	depth autopilot	(64) or (68)
3,4	heading autopilot	(64) or (68)
5,6	propulsion autopilot	(64) or (68)
7,8	roll autopilot	(64) or (68)
9 to 32	appendage control deflections	(58)
33 to 56	lump control deflections	(58)
57 to 62	RPM control	(56)
63 to 70	MBT blown volume	(86)
71 to 79	mass of HP air released per BG	(70)
80 to 87	mass of floodwater per WTC	(87)
88 to 93	u, v, w, p, q, r	(95)
94 to 96	x_0, y_0, z_0	(99)
97 to 99	ψ, θ, ϕ	(102)
100 to 103	e_0, e_1, e_2, e_3	(106)

18 MLD Curve Simulation

DSSP50 assumes a conventional Manoeuvering Limitation Diagram (MLD) as shown in the schematic of figure 17; however, it may not apply to unorthodox control arrangements. An overview of conventional MLDs is given in reference [43]. Safe operating envelopes are bounded on the left by a flood recovery curve or zero speed, and on the right by sternplane jam recovery curves. The upper and lower segments of the jam recovery curves are for jam to rise and jam to dive respectively. Between them there may be a segment where the allowable pitch limit is exceeded.

The curves are determined by the success or failure of a prescribed recovery scenario for a given combination of depth, speed, and other initial conditions. The scenario for recovery from a flood includes:

- size and location of the flooding hole,
- criteria for flood detection,
- time delays for recovery action,
- selection of autopilot or manual plane control for recovery,
- increasing RPM,
- blowing MBTs,
- optional loss of power, and
- optionally securing the flood (a secured *vs* unsecured flood).

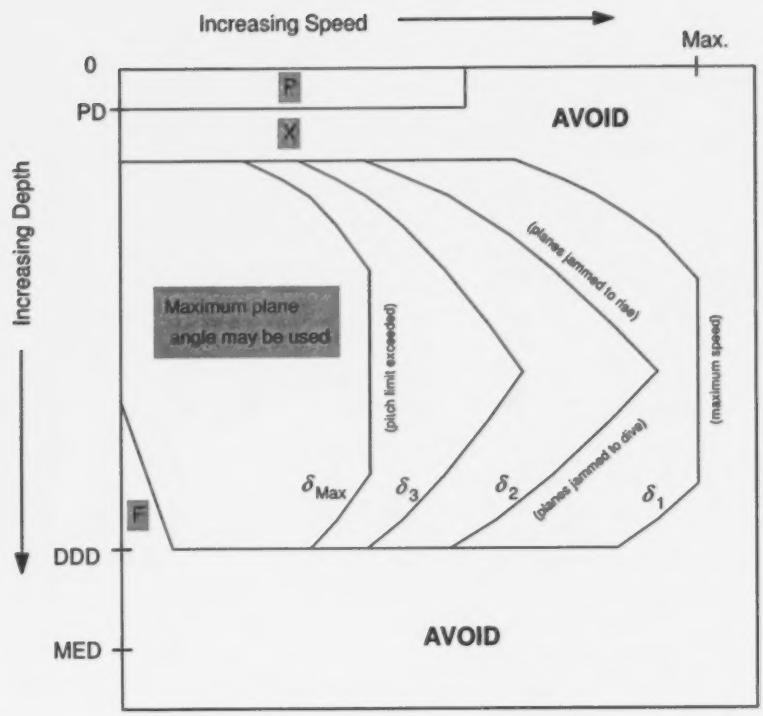

Figure 17 Schematic Manoeuvering Limitation Diagram.

Speed:	Max.	maximum submerged speed
Depth:	PD	periscope depth
	DDD	deep diving depth
	MED	maximum excursion depth
Operating Regions:	F	flood avoid zone (FAZ)
	P	transition from periscope depth to surface only
	X	avoid where deep draft surface vessels operate
Parameters:	$\delta_i,\ i = 1, 2, 3, \text{Max}$	magnitude of plane deflection, $\delta_1 < \delta_2 < \delta_3 < \delta_{\text{Max}}$

The scenario for recovery from a jam includes:

- the jammed appendage(s) and jam angle,
- time delays for jam recognition and subsequently for recovery actions,
- selection of autopilot or manual plane control for recovery,
- decreasing or reversing RPM,
- optional rudder deflection,
- optionally blowing and venting MBTs, and
- optionally unjamming the planes (a temporary *vs* permanent jam).

Successful flood recovery consists of reaching the surface and successful jam recovery consists of reducing speed to a prescribed value, in each case before a failure condition is encountered. For both, exceeding maximum depth (generally the MED, figure 17), exceeding the pitch limit, or (unlikely) exceeding the roll limit constitutes failure. For a flood, $u \leq 0$ constitutes failure, and for a jam, rising above minimum depth (typically PD or the surface) constitutes failure. By default, exceeding the run time limit before any of these conditions are met is also a failure, although that can be changed by the user.

DSSP50 calculates the MLD curves by stepping through a range of depths. The recovery boundary at each depth is found by successive bisection of speed. A free manoeuver based on the recovery scenario is internally generated for the current speed, and the range for the next bisection is determined by success or failure of the run. Several hundred free runs may be generated per curve, so a MLD simulation typically takes minutes, rather than seconds, to execute. MLD simulation input is described in section 29 of reference [2].

19 Concluding Remarks

This is the last of three documents describing build 090910 of the underwater vehicle manoeuvering simulation code DSSP50. It is the algorithm description, which provides an overview of the numerical methods in the code, and is intended for both users and code maintainers. Since much of the discussion can be read as a review of submarine hydrodynamics and systems modeling, the report may also be of interest to a wider audience.

There are still some capabilities, such as near-bottom operation, that can be added to the program. Others may undergo improvement or additional validation. Nevertheless, the current build is sufficiently complete to be benchmarked at this point before further development.

This page intentionally left blank.

References

For proprietary and other reasons, references denoted Limited Distribution are not for public release.

1. Mackay, M. (2009). DSSP50 Build 090910 Documentation, Part 1: Guide and Tutorial. (DRDC Atlantic TM 2009-226). Defence R&D Canada – Atlantic.

2. Mackay, M. (2009). DSSP50 Build 090910 Documentation, Part 2: Input Reference. (DRDC Atlantic TM 2009-227). Defence R&D Canada – Atlantic.

3. Abkowitz, M.A. (1972). *Stability and Motion Control of Ocean Vehicles* (second printing). Cambridge MA: MIT Press.

4. Watt, G.D. (1988). Estimates for the Added Mass of a Multi-Component, Deeply Submerged Vehicle, Part I: Theory and Program Description. DREA TM 88/213. Defence Research Establishment Atlantic.

5. Bohlmann, H.J. (1991). An Analytical Method for the Prediction of Submarine Manoeuvrability. In *RINA Warship '91 Symposium: Naval Submarines 3.* London: Royal Institution of Naval Architects.

6. Mackay, M. (1995). Estimation of the Force due to a Submarine Sail or Similar Appendage. In *Third Canadian Marine Hydrodynamics and Structures Conference.* Halifax: Technical University of Nova Scotia.

7. Gertler, M. and Hagen, G.R. (1967). Standard Equations of Motion for Submarine Simulation. NSRDC Report 2510. Naval Ship Research and Development Center.

8. Mackay, M. (2006). Estimating the In-Plane Hydrodynamic Loads on a Submarine Hull at Incidence. DRDC Atlantic TM 2006-020. Defence R&D Canada – Atlantic.

9. Hooft, J.P. (1986). Hydrodynamic Forces on Tear-Drop Bodies. MARIN Report No. 07659–1–MO. Maritime Research Institute Netherlands. Limited Distribution.

10. Ward, B. and Lloyd, A.J.R.M. (1990). Experiments to Measure Forces and Moments on Bodies of Revolution of Various Fineness Ratios in Rectilinear Flow. ARE TR90308. Admiralty Research Establishment. Limited Distribution.

11. Jeans, T.L. (2007). *An Estimation Method for the Normal Force Distribution on Slender Axisymmetric Bodies with Tapered Tails.* Ph.D. Thesis, University of New Brunswick.

12. Mackay, M. (2003). The Standard Submarine Model: A Survey of Static Hydrodynamic Experiments and Semiempirical Predictions. DRDC Atlantic TR 2003-079. Defence R&D Canada – Atlantic.

13. Comstock, J.P. (1967). *Principles of Naval Architecture* (second edition). New York: Society of Naval Architects and Marine Engineers.

14. Hoerner, S.F. (1958). *Fluid-Dynamic Drag.* Midland Park, NJ: published by the author.

15. Mackay, M. (1995). A Review of Semiempirical Methods for Predicting Appendage Forces. DREA Report 95/102. Defence Research Establishment Atlantic. Limited Distribution.

16. Aucher, M. (1981). Dynamique des Sous-Marins. From *Sciences et Techniques de l'Armement, 4^e fascicule.* Paris: Imprimerie Nationale.

17. Etkin, B. (1972). *Dynamics of Atmospheric Flight.* New York: Wiley.

18. Hoerner, S.F. and Borst, H.V. (editor) (1975). *Fluid-Dynamic Lift.* Brick Town, NJ: published by Mrs. L.A. Hoerner.

19. Lyons, D.J. and Bisgood, P.L. (1945). An Analysis of the Lift Slope of Aerofoils of Small Aspect Ratio, including Fins, with Design Charts for Aerofoils and Control Surfaces. ARC R&M 2308. Aeronautical Research Council.

20. Abbott, I.H. and von Doenhoff, A.E. (1959). *Theory of Wing Sections.* New York: Dover.

21. Duncan, W.J., Thom, A.S., and Young, A.D. (1974). *Mechanics of Fluids* (second edition). Melbourne: Edward Arnold (Australia).

22. Mackay, M., Bohlmann, H.J., and Watt, G.D. (2002). Modeling Submarine Tailplane Efficiency. In *Challenges in Dynamics, System Identification, Control and Handling Qualities for Land, Air, Sea, and Space Vehicles.* (RTO–MP–095). Paris: NATO RTO.

23. Nonweiler, T. (1954). The Effect of the Hull of a Submarine on the Lift Forces Developed by Hydroplanes. AEW(Haslar) Report No. 56/54. Admiralty Experiment Works.

24. Dempsey, E.M. (1977). Static Stability Characteristics of a Systematic Series of Stern Control Surfaces on a Body of Revolution. DTNSRDC Report 77–0085. David Taylor Naval Ship Research and Development Center.

25. Spreiter, J.R. (1950). The Aerodynamic Forces on Slender Plane- and Cruciform-Wing and Body Combinations. NACA Report 962. National Advisory Committee for Aeronautics.

26. Albone, C.M. (1972). Fortran Programs for Axisymmetric Potential Flow around Closed and Semi-Infinite Bodies. ARC CP–1216. Aeronautical Research Council.

27. Truckenbrodt, E. (1955). A Method of Quadrature for Calculation of the Laminar and Turbulent Boundary Layer in case of Plane and Rotationally Symmetric Flow (translation). NACA Technical Memorandum 1379. National Advisory Committee for Aeronautics.

28. Mackay, M. (2004). A Review of Submarine Out-of-Plane Normal Force and Pitching Moment. DRDC Atlantic TM 2004-135. Defence R&D Canada – Atlantic.

29. van Lammeren, W.P.A., van Manen, J.D., and Oosterveld, M.W.C. (1969). The Wageningen B–Screw Series. *SNAME Transactions*, Vol. 77. New York: Society of Naval Architects and Marine Engineers.

30. Brockett, T.E. (1998). Propulsor Design for an Unmanned Underwater Vehicle: 30/26 Open C/R for Dolphin Mk II. DREA CR 98/418. Defence Research Establishment Atlantic. Limited Distribution.

31. Mackay, M. (1992). DREA Submarine Simulation Program Version 0.2 (DSSP02) — Release Notes. DREA TC 92/308. Defence Research Establishment Atlantic. Limited Distribution.

32. Mackay, M. (2001). Some Effects of Tailplane Efficiency on Submarine Stability and Manoeuvering. DREA TM 2001–031. Defence Research Establishment Atlantic.

33. Van Wylen, G.J. and Sonntag, R.E. (1976). *Fundamentals of Classical Thermodynamics* (second edition). New York: Wiley.

34. Itard, X. (1999). Recovery Procedure in case of Flooding. In *RINA Warship '99 Symposium: Naval Submarines 6.* London: Royal Institution of Naval Architects.

35. Rogers, G. and Mayhew, Y. (1992). *Engineering Thermodynamics Work and Heat Transfer* (fourth edition). New York: Wiley.

36. Strumpf, A. (1960). Equations of Motion of a Submerged Body with Varying Mass. SIT Report DL–60–9–771. Stevens Institute of Technology.

37. Imlay, F.H. (1961). The Complete Expressions for "Added Mass" of a Rigid Body moving in an Ideal Fluid. DTMB Report 1528. David Taylor Model Basin.

38. Press, W.H., Teukolsky, S.A., Vetterling, W.T., and Flannery, B.P. (1992). *Numerical Recipes in Fortran*, Second Edition. Cambridge: CUP.

39. Phillips, W.F., Hailey, C.E., and Gebert, G.A. (2000). A Review of Attitude Kinematics for Aircraft Flight Dynamics. (AIAA paper 2000–4302). In: *AIAA Modeling and Simulation Technologies Conference, Denver, CO*. American Institute of Aeronautics and Astronautics.

40. Enright, W.H., Jackson, K.R., Nørsett, S.P., and Thomsen, P.G. (1986). Interpolants for Runge-Kutta Formulas. *ACM Transactions on Mathematical Software*, Vol. 12, No. 3. Association for Computing Machinery.

41. Enright, W.H., Jackson, K.R., Nørsett, S.P., and Thomsen, P.G. (1988). Effective Solution of Discontinuous IVPs Using a Runge-Kutta Formula Pair with Interpolants. *Applied Mathematics and Computation*, Vol. 27. Amsterdam: Elsevier.

42. McCalla, T.R. (1967). *Introduction to Numerical Methods and Fortran Programming.* New York: Wiley.

43. Haynes, D., Bayliss, J., and Hardon, P. (2002). Use of the Submarine Research Model to Explore the Manoeuvring Envelope. In *RINA Warship 2002 Symposium: Naval Submarines 7.* London: Royal Institution of Naval Architects.

List of symbols/abbreviations/acronyms/initialisms

In almost all cases, we have kept the nomenclature used in the cited references. Consequently a number of symbols have more than one interpretation; the correct one will be apparent from the context.

Nondimensionalization follows the standard convention:

$$b'_e = \frac{b_e}{\ell}, \quad Z' = \frac{Z}{\frac{1}{2}\rho\ell^2U^2}, \quad \text{etc.}$$

Symbols

a_e	effective aspect ratio
$\mathbf{A}$	added mass matrix
A_{base}	hull base area
A_{wet}	hull wetted area
b	semispan of isolated appendage, or measured from hull centerline
b_d, b_{de}	deck height from centerline, effective deck height
b_{ep}	spanwise location of endplate
b_{exp}	exposed appendage span
b_{sp}	spanwise location of sailplanes on the sail
b_1, b_2	spanwise location of inboard and outboard flap extent
B	buoyancy force; hull breadth
B_{ch}, B_{ct}	compression buoyancy loss for hull and tiles
$c, \overline{c}$	appendage chord, mean chord
$\overline{c_f}$	mean flap chord
c_l	leading edge chordwise coordinate
$\mathbf{C}_i$	loads on vehicle component i
$\mathbf{C}_{i,j}$	interaction loads for vehicle components i and j
C_C	autopilot control gain
C_E	autopilot error gain
C_F	hull friction drag coefficient; flooding coefficient of discharge
C_{pr}	gain to correct for plane reversal
C_P	prismatic coefficient
C_{Pb}	spanwise location of center of pressure
C_{Pc}	chordwise location of center of pressure
C_Q^*, C_T^*	torque and thrust coefficients for Wageningen B data
C_X, C_Z	appendage axial and normal force coefficients
C_{X_j}	appendage junction axial force coefficient
$C_{Zp'}$	appendage normal force roll derivative

$C_{Z\alpha}$	appendage linear normal force coefficient
$C_{Z\alpha(ep)}$	all-moving appendage: $C_{Z\alpha}$ with endplate corrections
$C_{\Delta f}$	hull residual drag coefficient
$\mathbf{D}_k$	loads on lump k
D_F	flooding breach diameter
D_P	propeller diameter
D'_0	zero-incidence drag
e_0, e_1, e_2, e_3	quaternions (Euler-Rodrigues parameters)
f	appendage camber; dihedral factor; OOP load distribution function
f_1, f_2	parameter fitting functions for tailplane efficiency
$\mathbf{F}$	hydrodynamic load vector
g	gravitational acceleration
$\mathbf{G}$	gravity and buoyancy load vector
h, h'	total endplate height, endplate height from attachment
$\mathbf{I}$	inertial matrix
$I_x, \ldots, I_{xy}, \ldots$	moments and cross products of inertia
J	factor for twist-induced lift
J_C	autopilot control signal
J_E, J'_E	autopilot error signal, damped autopilot error signal
k	out-of-plane load distribution parameter; Nonweiler's $\phi/(\pi/2)$
k_1, k_2	PID autopilot error damping equation coefficients
k_{ep}, k'_{ep}	endplate factor for appendage, and for the plate itself
k_r	hull roughness allowance
k_s	sail factor
k_{sp}	sailplane angle of attack correction factor
k_{WB}	tailplane efficiency for a control deflection
k_n	coefficient model propulsion state parameter
k_δ	appendage flap profile drag
$\mathbf{K}$	canonical matrix for the dynamic system
K, M, N	roll, pitch, and yaw moment
K_P, K_I, K_D	PID autopilot coefficients
K_T	propulsor thrust coefficient
K_Q	propulsor torque coefficient
K_{WB}	tailplane efficiency for incidence
ℓ	reference length for nondimensionalizing, typically LBP
$\mathbf{L}$	earth to body axis transformation matrix; momentum vector
L/D	slenderness ratio
l_z	depth autopilot lookahead distance
$l_1, \ldots, n_3$	elements of transformation matrix $\mathbf{L}$
m	mass; index of OOP load distribution function
$\mathbf{M}$	inertial plus added mass matrix

m_{BT}	mass of air blown into MBT
m_{HP}	mass of HP air released
m_F	mass of flood water
n	propulsor revolutions
O_C	WTC occupancy
p, q, r	roll, pitch, and yaw rate
$\mathbf{P}$	propulsion vector
P	power, pressure
P_{BT}, P_{HP}	ballast tank (ambient) pressure, bottle group pressure
$P_X, \ldots, P_N$	propulsion vector elements
$\mathbf{Q}$	general load vector
Q	propulsion torque
r	local hull radius
R	ideal gas constant; slope fitting function for tailplane efficiency
r_{te}	radius at appendage trailing edge
r'_P	critical pressure ratio
S	lift reference area
$\mathbf{S}$	balance load vector
S_{exp}	exposed appendage area
S_m	area of moving part of all-moving appendage
t	time; appendage thickness
T	thrust
$\mathbf{T}$	axis rotational load vector
T_{BT}, T_{HP}	ballast tank temperature, bottle group temperature
$\mathbf{u}$	state vector or extended state vector
u, v, w	axial, lateral, and normal velocity
U	total velocity
$U_{c\delta}$	sternplane reversal speed
$\mathcal{V}$	specific volume
V_{BT}, V_{HP}	ballast tank volume, bottle group volume
W	weight
x, y, z	reference axis, local axes
X, Y, Z	axial, lateral, and normal forces
x_{AP}	x for aft perpendicular
x_B, y_B, z_B	center of buoyancy coordinates
x_{ch}, x_{ct}	axial location of hull and tile compression loss
x_G, y_G, z_G	center of gravity coordinates
x_{TE}	x at the sail trailing edge
x_0, y_0, z_0	coordinates in earth-fixed axes
x_1, x_2	ends of the OOP load distribution function
$X_\bullet, \ldots, N_\bullet$	initial buoyancy and trim loads

$\mathbf{Y}$	total dynamic system vector
Y_{sail}	sideforce on sail
z_{0BT}	reference depth for ballast tank
z_{0F}	reference depth for flood
z_{ch}, z_{ct}	depth for hull and tile compression loss
Z_W	normal force on an isolated appendage ('wing')
Z_{WB}	incremental normal force for a tail appendage
$Z_{W(B)}$	force on a wing in the presence of a body
$\widehat{Z}$	OOP normal force distribution on hull afterbody
α	angle of attack; phase lead autopilot amplitude gain
α_b	appendage geometric twist
α_g	equivalent α for camber and twist
$\alpha_\bullet$	augmented angle of attack
$\alpha_{\bullet(0)}$	control deflection component of $\alpha_\bullet$
$\alpha_{\bullet(\alpha)}$	geometric incidence component of $\alpha_\bullet$
β	angle of drift; propeller hydrodynamic pitch angle
β_c	critical drift angle
γ	tail cone angle; ratio of specific heats
δ	control surface deflection
δ_e	effective flap angle of deflection
δ^*	boundary layer displacement thickness
ζ_n	RPM rate damping
ζ_δ	control deflection damping
η	appendage flap gap correction
θ	pitch angle
λ	taper ratio
ξ	nondimensional axial coordinate
ρ, ρ_{air}	density of water, air
$\overline{\rho}_{air}$	net density of air in MBT
σ	spanwise flap efficiency; leading edge spanwise coordinate
σ_1, σ_2	inboard/outboard components of σ
τ	chordwise flap efficiency; phase lead anticipation; convection time
ϕ	roll angle; appendage anhedral or dihedral angle
ψ	yaw angle or heading
ω_n	RPM rate frequency
ω_δ	control response frequency
$\Omega_{c/2}$	appendage mid-chord sweep
$\mathbf{\Omega}$	vector angular velocity vector

Subscripts

c	commanded value
$\bullet$	initial value; augmented value

Coordinate System

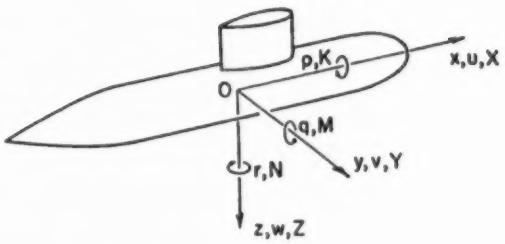

Incidence angles: $\alpha = \tan^{-1}(w/u)$, $\beta = \tan^{-1}(-v/u)$.

Acronyms

AP	Aft Perpendicular
BG	Bottle Group
CB	Center of Buoyancy
CFD	Computational Fluid Dynamics
CG	Center of Gravity
DDD	Deep Diving Depth
G&H	Gertler and Hagen (reference [7])
HP	High Pressure
LBP	Length Between Perpendiculars
MBT	Main Ballast Tank
MED	Maximum Excursion Depth
OOP	Out-Of-Plane
PD	Periscope Depth
PID	Proportional-Integral-Derivative (control)
UUV	Unmanned Underwater Vehicle
WTC	WaterTight Compartment

This page intentionally left blank.

Distribution

DRDC Atlantic TM 2009–228

LIST PART 1: Internal Distribution by Center:

2 Author (1 hard copy, 1 CD)

3 DRDC Atlantic Library (1 hard copy, 2 CDs)

5 TOTAL LIST PART 1

LIST PART 2: External Distribution within Canada by DRDKIM

1 Library and Archives Canada

1 NDHQ/DRDKIM 3

1 NDHQ/DMSS 2

1 NDHQ/DMEPM (SM) 4–2

1 CFMWC – Attn: N. Sponagle
PO Box 99000 STN Forces, Halifax NS, B3K 5X5

1 Micromedia Limited, Acquisitions/Research Indexes
20 Victoria St., Toronto ON, M5C 2N8

1 NRC Institute for Ocean Technology – Attn: Director General
PO Box 12093 Station A, St. John's NL, A1B 3T5

7 TOTAL LIST PART 2

LIST PART 3: External Distribution outside Canada by DRDKIM

1 Defence Research Information Center
Station Square House, St. Mary Cray, Orpington Kent, England BR5 3R3

1 DPA
Ash 3c #3311, MOD Abbey Wood, Bristol, England BS34 9JH

1 MoD – Attn: Director of Naval Architecture and Marine Engineering
PO Box 20702, 2500 ES The Hague, The Netherlands

1 MARIN – Attn: Head of Naval Research
PO Box 28, 6700 AA Wageningen, The Netherlands

1 Navy Office – Attn: Director Naval Ship Design
Department of Defence CP1–505, Canberra ACT 2600, Australia

1 Document Exchange Center, Defence Information Services Branch
Department of Defence CP2–5–08, Canberra ACT 2600, Australia

1 Bundesamt für Wehrtechnik und Beschaffung – SG 13
Postfach 7360, 6057 Koblenz, Germany

---

7 TOTAL LIST PART 3

LIST PART 4: External Distribution outside Canada by DRDC Atlantic

3 Under covering letter from Canadian Project Officer, IEP ABCA–02–01:

NSWCCD – Attn: David Walden, Project Officer ABCA–02–01
9500 MacArthur Blvd, Bethesda MD, USA 20817–5700

DSTL Winfrith – Attn: Simon Tinker, Project Officer ABCA–02–01
Bldg A32 Winfrith Technology Center, Dorchester Dorset, England DT2 8WX

DNPD – Attn: Martin Grimm, Project Officer ABCA–02–01
Department of Defence CP4–5–074, Canberra ACT 2600, Australia

---

3 TOTAL LIST PART 4

---

22 **TOTAL COPIES REQUIRED**

DOCUMENT CONTROL DATA		
1. ORIGINATOR Defence R&D Canada – Atlantic	2. SECURITY CLASSIFICATION Unclassified	
3. TITLE DSSP50 build 090910 Documentation, Part 3: Algorithm Description		
4. AUTHORS M. Mackay		
5. DATE OF PUBLICATION December 2009	6a. NO. OF PAGES 70	6b. NO. OF REFS 43
7. DESCRIPTIVE NOTES DRDC Atlantic Technical Memorandum		
8. SPONSORING ACTIVITY		
9a. PROJECT OR GRANT NO. 11GX01	9b. CONTRACT NO.	
10a. ORIGINATOR'S DOCUMENT NUMBER DRDC Atlantic TM 2009–228	10b. OTHER DOCUMENT NOS.	
11. DOCUMENT AVAILABILITY Unlimited		
12. DOCUMENT ANNOUNCEMENT (if different from 11)		
13. ABSTRACT DSSP50 is a computer code for evaluating the dynamics and manoeuverability of submarines and smaller streamlined underwater vehicles. This document is a description of the algorithms used in the program. Although written for DSSP50, it may be useful to those with a more general interest in simulating submarine manoeuvers. Other documents provide a guide to using DSSP50 and detail its input requirements.		
14. KEYWORDS Underwater Vehicles Submarines Manoeuvering Simulation		

This page intentionally left blank.

This page intentionally left blank.

Defence R&D Canada

Canada's leader in defence
and National Security
Science and Technology

R & D pour la défense Canada

Chef de file au Canada en matière
de science et de technologie pour
la défense et la sécurité nationale

www.drdc-rddc.gc.ca